scientific reports

OPEN

Advanced methodology for maximum torque point tracking of hybrid excitation PMSM for EVs

Mahmoud M. Elymany[1], Nadia A. Elsonbaty[1], Aymen FLah[2,3,4], Lukas Prokop[5], Habib Kraiem[6]✉, Mohamed A. Enany[1] & Ahmed A. Shaier[1]

This manuscript presents an innovative control strategy for the Hybrid Excitation Permanent Magnet Synchronous Motor (HEPMSM) designed for electric vehicle (EV) applications. The strategy combines Maximum Torque Point Tracking (MTPT) and Maximum Torque Per Ampere (MTPA) techniques to track the ideal torque-speed profile, ensuring maximum torque at low speeds for starting and climbing, and high power at higher speeds for cruising. A novel unidirectional excitation current method is proposed to replace traditional bidirectional field current control, eliminating the risk of permanent magnet demagnetization, reducing copper losses, and increasing efficiency. This approach extends the constant power (CP) region by a 4.2:1 ratio. The manuscript also introduces a detailed mathematical model, considering both iron core losses and their impact on the EV profile. Additionally, the Multi-Objective Ant Lion Optimizer (MOALO) algorithm is used in two stages: first to optimize the hybridization ratio (HR) and base speed (N_b), and second to analyze the effect of varying the hybridization ratio while maintaining constrained output power. The proposed strategy is validated through MATLAB simulations, demonstrating its effectiveness in achieving high acceleration, efficiency, and reliability for EV applications.

Keywords Hybrid excitation permanent magnet synchronous motor, Electric vehicle, Hybridization ratio, Ant lion optimization algorithm

The integration of AC motors in electric vehicles (EVs) represents a key milestone in automotive history, driven by their technological development and ability to fulfill the needs of EVs. The shift to AC motors for EVs began after the realization of their performance superiority in certain areas over DC motors, which were initially used in early prototypes of EVs[1]. Before World War II, both Europe and the United States saw extensive use of electric cars powered predominantly by DC motors due to simpler control mechanisms. However, advances in AC motor technology, combined with improvements in power electronics, enabled their integration into modern EVs[2]. Three primary types of AC motors are considered for EV applications: induction motors (IMs), permanent magnet synchronous motors (PMSMs), and switched reluctance motors (SRMs). IMs are known for their robustness, reliability, and cost-effectiveness, as they do not require rare earth materials, and they can operate at high speeds. However, they tend to consume more energy at lower speeds and have lower torque efficiency compared to PMSMs[3]. PMSMs, on the other hand, offer high efficiency and torque at lower speeds, a compact size, and an excellent power-to-weight ratio. Their main drawbacks are the reliance on rare earth materials, making them costly, and the environmental concerns associated with material extraction[4]. SRMs are recognized for their simple, rugged construction and high fault tolerance, making them lower in cost and with minimal reliance on rare earth materials. However, they face challenges such as high noise and vibration levels and require more complex control systems[5]. One of the main challenges in EVs is choosing the most efficient motor that aligns with the vehicle's unique needs. The motor drive system is crucial, as it determines the motor's performance for the intended use. A summary of different EV motor drive systems and strategies can be found in[6].

[1]Electrical Power and Machines Department, Faculty of Engineering, Zagazig University, Zagazig 44519, Egypt. [2]Processes, Energy, Environment, and Electrical Systems, National Engineering School of Gabès, University of Gabès, Gabès, Tunisia. [3]Centre for Research Impact & Outcome, Chitkara University Institute of Engineering and Technology, Chitkara University, Rajpura 140401, Punjab, India. [4]Applied Science Research Center, Applied Science Private University, Amman 11931, Jordan. [5]ENET Centre, CEET, VSB-Technical University of Ostrava, Ostrava 708 00, Czech Republic. [6]Center for Scientific Research and Entrepreneurship, College of Engineering, Northern Border University, 73213, Arar, Saudi Arabia. ✉email: ahmshaier@gmail.com

PMSMs offer significant advantages for EVs, such as their ability to handle multivariable, nonlinear, and strongly coupled systems, which contribute to their high performance. However, they also present several challenges, particularly their reliance on rare earth materials like neodymium and dysprosium for the magnets. These materials are expensive, subject to supply chain uncertainties, and raise environmental and ethical concerns due to the destructive nature of their extraction processes. This reliance also makes PMSMs more costly than other motor types, which can increase the overall price of EVs. Moreover, the extraction of rare earth elements can result in considerable environmental harm, including habitat destruction and pollution[7]. Additionally, over time, the magnets in PMSMs may experience magnetic field degradation, particularly at high temperatures, which can reduce motor efficiency and performance.[8]. PMSMs also lack the wide constant power (CP) operating range required by EVs. Various control methods, such as predictive control, state feedback control, finite position set, and sliding mode control, have been explored to overcome these limitations in EV applications[9]. In contrast, conventional field coil motors, such as wound field synchronous motors, have efficiently met EV requirements both numerically and experimentally, aided by their field current control, but they face challenges of lower efficiency, larger size, and poorer torque density compared to PMSMs. These comparative challenges highlight the need for alternative materials, improved manufacturing processes, sustainable mining practices, and advancements in motor design to reduce environmental impact and enhance the durability, efficiency, and cost-effectiveness of PMSMs while addressing the size and torque limitations of field coil motors.

Hybrid Excitation Permanent Magnet Synchronous Motors (HEPMSMs) are an excellent candidate for EVs due to their unique flexibility in dynamically controlling magnetic flux. By combining the advantages of two excitation systems, HEPMSMs address challenges associated with traditional motor designs[10]. These motors are typically integrated into the EV powertrain, either as hub motors directly mounted in the wheels or centrally installed and connected to the axle via a transmission. The motor utilizes a dual excitation system comprising permanent magnets for a base magnetic field and controllable windings for electromagnetic excitation. This configuration requires advanced power electronics and controllers to manage the hybrid excitation system effectively. Due to the variable flux densities introduced by hybrid excitation, robust thermal management systems, such as liquid or air cooling, are essential to ensure efficient heat dissipation. Additionally, a dedicated control unit coordinates the motor's hybrid excitation components, optimizing performance by balancing contributions from both the magnet-based and winding-based excitation sources[11]. HEPMSMs can be categorized based on the placement of the excitation sources: some designs feature sources located in the stator, others in the rotor, while a hybrid arrangement includes permanent magnets in the rotor and excitation windings in the stator. During operation, HEPMSMs leverage the permanent magnets for a steady base magnetic field and dynamically adjust the flux through the controllable excitation winding to meet varying speed and load requirements. This capability enables high efficiency across diverse driving conditions.[12]. The ability to dynamically regulate excitation allows HEPMSMs to handle variable loads more effectively than conventional motors, making them highly suitable for both urban stop-and-go traffic and high-speed highway driving. Furthermore, the dual excitation design enhances reliability by providing redundancy; the motor can continue functioning even if one excitation source (e.g., the winding or magnet) fails. This combination of efficiency, adaptability, and fault tolerance makes HEPMSMs a compelling choice for modern EVs. Generally, placing the excitation winding in the stator is preferred to prevent issues related to sliding contact, such as the need for slip ring maintenance and the risk of brush sparking[13].

Vector control, or field-oriented control (FOC), is commonly used for HEPMSMs because it allows for accurate control of flux and torque. By independently managing the d-axis (magnetizing flux) and q-axis (torque production), it ensures smooth operation in dynamic conditions. Recent research indicates that vector control is effective in dynamically optimizing the hybrid excitation system, leading to improved performance of the EV powertrain[14]. Maximum torque control strategies optimize the torque output by adjusting field currents through self-optimizing methods. This is particularly beneficial for HEPMSMs in high-speed and high-load conditions. These strategies have been shown to enhance power output and system efficiency[15]. The advantages of hybrid excitation topologies and control strategies for stator permanent magnet machines in DC power systems are summarized in[16], while flux-weakening control methods for HEPMSMs are explored in[17]. Additionally, a parallel double excitation magnetic equivalent circuit model for unipolar HEPMSMs using the hybrid excitation strategy is discussed in[18]. An optimized HEPMSM featuring a salient pole magnet shunting rotor is proposed to demonstrate a maximum torque control strategy with zero d-axis currents[19]. The extension of the CP speed range through various HEPMSM designs is also discussed. The structural topology and operating principle of an EV motor prototype are presented and analyzed in[20]. Flux weakening control is critical for HEPMSMs operating at high speeds, where the back-electromotive force (EMF) may exceed the inverter voltage limit. This method strategically reduces the magnetic flux to prevent over-saturation while maintaining efficiency. Studies highlight its role in extending operational speed ranges[21]. In[22], the authors introduced three innovative rotor design concepts for HESMs to enhance density and flux regulation capabilities. Additionally, a permanent magnet motor with hybrid PM excitation and an asymmetric rotor structure for improved torque performance is proposed in[23]. Model predictive control (MPC) employs predictive algorithms to manage system dynamics efficiently, enabling real-time adjustments to the hybrid excitation system and enhancing performance under varying driving conditions. Studies show that MPC delivers faster response times and reduces torque ripple, making it an excellent choice for controlling HEPMSMs[24]. Direct torque control (DTC) allows for direct management of torque and flux without the need for complex coordinate transformations. Although it is simpler than field-oriented control (FOC), it may lead to increased torque ripple. Recent advancements in DTC for HE-PMSMs have shown enhancements in transient response and fault tolerance[25].

System-level optimization in EVs aims to enhance both motor performance and overall efficiency by considering the interaction between permanent magnet (PM) excitation and wound excitation to maximize power density while minimizing losses. For example, research on three-wheel EVs has demonstrated improvements in energy efficiency through system-level optimizations[26]. Multi-objective design optimization seeks to balance factors such as efficiency, torque density, thermal management, and material cost. A study on hybrid excitation double-stator PM machines emphasized the importance of optimizing both stator and rotor designs for better EV performance[27]. Finite Element Analysis (FEA) is frequently used to refine the electromagnetic properties of HEPMSMs by simulating magnetic fields and losses, leading to improved motor designs that boost traction performance, as shown in research on hybrid excitation synchronous machines with magnetic shunting rotors[28]. Loss optimization control strategies focus on minimizing copper and iron losses, particularly in in-wheel EV systems, thereby improving overall efficiency[29]. Topology optimization involves designing innovative rotor and stator configurations to enhance torque production and reduce material usage, with dual-direction hybrid excitation topologies improving flux regulation and efficiency in EV motors[15]. Thermal and mechanical design optimizations aim to improve heat dissipation to avoid efficiency losses due to overheating and ensure the motor's durability under varying operational conditions, as seen in the optimization of brushless synchronous machines with wound-field excitation for hybrid electric vehicles[30]. Lastly, field current optimization methods dynamically adjust excitation winding currents to maximize performance under different loads, with self-optimizing algorithms developed for real-time field current control of HE-PMSMs during driving[14]. Optimization methods for HEPMSMs have evolved significantly, offering enhanced precision, efficiency, and adaptability. Classical approaches such as the Grey Wolf Optimization (GWO) algorithm, based on state feedback control, have demonstrated faster response times compared to traditional PI controllers[31]. Another optimization technique targets the hybridization ratio (HR), a critical factor influencing motor performance, by reducing overdesign in the drivetrain and improving efficiency[32,33]. Bio-inspired population-based algorithms like the Ant Lion Optimizer (ALO) approximate optimal solutions through iterative refinement. A Despite their strengths, traditional methods face challenges, such as nonlinear dependencies of excitation flux on excitation current (I_f), which can lead to improper current distribution and false excitation values in prototypes[34].Real-time particle swarm optimization (PSO) offers accurate parameter identification, improving performance by optimizing excitation currents[35]. The Taguchi method, validated experimentally, reduces variations and ensures robust performance in diverse operating conditions[36]. Additional contributions include research in[37], which focuses on torque improvements through hybrid excitation, and the study in[38], which introduces advanced DTC methods for HEPMSMs to improve dynamic performance. These modern methods surpass earlier techniques, leveraging advanced simulations, bio-inspired algorithms, and data-driven strategies for optimal motor design and control in EV applications. The main innovative contributions of this work are outlined as follows:

- This work provides analytical expressions for tracking the ideal EV torque-speed profile using both Maximum Torque Point Tracking (MTPT) and Maximum Torque Per Ampere (MTPA) strategies. The first key advantage is preventing motor operation in its natural mode ($T\,\alpha\,\frac{1}{N_r^2}$), thereby expanding the constant power (CP) range, improving reliability, and ensuring fast torque response for EV drives. The second advantage is minimizing copper losses to enhance motor efficiency. Unlike other control strategies, the proposed method achieves a perfect linear relationship between excitation current, excitation flux, and torque-producing flux.
- This study utilizes a unidirectional, non-reversible electric field current that continuously supports the PM field throughout the entire EV operating range, facilitating a smooth transition from the CT to CP region, reducing harmonics, enhancing efficiency, and preventing demagnetization. In contrast, previous research relied on bidirectional field currents, first aiding the PM flux (positive) and then reversing to weaken it (negative).
- The proposed strategy enables an extended speed ratio of 4:1 beyond the constant power speed ratio (CPSR). This results in a linear relationship between stator current and torque, providing rapid response and stable torque control.
- The speed of the EV can vary significantly, ranging from very slow to very high, for the same accelerator position, depending on road conditions. Therefore, the proposed control methodology focuses on torque control rather than speed control, effectively preventing improper excitation current distribution and ensuring accurate excitation values.
- The computational processor (microcontroller) in the motor drive system incorporates a current distributor sub-module that divides the entire speed operation range into two regions: the CT and CP regions. This sub-module facilitates the selection between the MTPT algorithm and the efficiency maximization algorithm.
- The control strategy of the proposed method utilizes three current controllers for I_f, I_{sq}, and I_{sd}. Proper control of the I_f and I_{sq} current components ensures that the motor achieves the optimal characteristics required for the EV at each speed and under the ZDAC technique.
- The primary goal of improving inverter reliability and reducing costs is to ensure that, at low speeds, the volt-ampere increases linearly with speed, while staying constant within the CP region. Additionally, a key objective of high-performance control strategies (maintaining linear control over torque) has been successfully achieved.

- The analysis and methodologies presented in this manuscript have led to motor drive systems with the following benefits:
- Enhanced dynamics and improved performance.
- Cost reduction through optimal machine utilization.
- System optimization tailored to the specific application requirements.
- Protection of the motor from excessive power losses.
- Flexibility of the motor drive to adapt to various operating environments without the need for design modifications.
- Simple and efficient linear torque controllers suitable for motor drives across a wide speed range.

The remainder of the paper is structured as follows: Sect. "Proposed control strategies" discusses the operating principles of the HEPMSM, the concepts behind the proposed efficient control strategy, and the strategies applied for MTPA (Maximum Torque Per Ampere) and unidirectional electric field current. Section "ZDAC Based Steady State Mathematical Model". presents the ZDAC steady state-controlled mathematical model based on an insight HR with and without iron loss consideration. An illustrative phasor diagram is provided. In Sect. "Proposed EV-MTPT Strategy"., EV-MTPT performance characteristics with and without iron core resistance are illustrated, compared, and explained. EV-MTPT Control Implementation is demonstrated in Sect. "EV-MTPT Control Implementation". To evaluate the proposed control and modelling of the HEPMSM, an adaptive newly Multi-Objective Ant Lion Optimizer (MOALO)[39] is applied as given in Sect. "Simulation Modeling and Results". Due to the Lack of existence of the HEPMSM, simulation work is carried out to approve both the proposed mathematical model and MOALO searching algorithm as depicted in Sect. "Simulation Modeling and Results". Finally, Section "Conclusion and Future Works" summarizes the conclusion of this paper.

Proposed control strategies

The two torque-speed (T-N) profiles for electric motor drives in EVs differ in terms of performance characteristics and operational efficiency. Figure 1(a) features a constant torque (CT) region at low speeds, followed by a constant power (CP) region, with torque decreasing inversely with speed after the base speed (N_{base}). This profile is ideal for high-performance EVs requiring both strong acceleration and consistent power output over a wide speed range, suitable for acceleration and cruising. In contrast, Fig. 1(b) introduces a rated torque (T_{rated}) lower than the maximum torque (T_{max}), with a CT region transitioning to a reduced torque with constant power between N_{base} and N_{rated}, and further sharp torque reduction beyond N_{rated}, leading to decreased power. The term "speed ratio (α)" is defined as the ratio of the N_{max} to the N_{base}. A higher α results in a lower-power motor with reduced size, cost, and improved efficiency. This profile reflects motors constrained by thermal limitations or efficiency optimization, prioritizing long-distance cruising and sustained high-speed operation over maximum performance.

The primary objective of the control strategy is to track the torque-speed profile of the EV, referred to as the maximum torque point tracing (MTPT) profile. This profile is characterized by two distinct regions: a) a high-acceleration region where the motor operates at a constant maximum torque to provide optimal performance during rapid acceleration, and b) a wide constant power (CP) region, where the torque decreases inversely with speed to ensure efficient utilization of the motor's capabilities. This approach avoids operation within the motor's normal mode to enhance overall efficiency and performance. Given that the motor under consideration exhibits inverse saliency ($L_q > L_d$), with only a minimal difference between the L_q and L_d inductances, the motor can be approximated as a non-salient machine. This characteristic simplifies the control design, allowing the implementation of techniques such as Maximum Torque Per Ampere (MTPA) control or the $I_d = 0$ method, also referred to as the zero direct axis current (ZDAC) method. Both of these techniques focus on optimizing torque production while minimizing current consumption to improve energy efficiency[19,40]. Therefore, the proposed control strategy integrates three basic techniques to achieve superior motor performance and energy efficiency:

- **Tracking the EV *T-N* Profile (MTPT):** This ensures that the motor operates optimally across both constant torque and constant power regions, delivering high acceleration and efficient high-speed cruising.
- **Maximum torque per ampere (MTPA) or ZDAC technique:** By minimizing current usage for a given torque demand, this method enhances motor efficiency and reduces losses, making it suitable for motors approximated as non-salient.

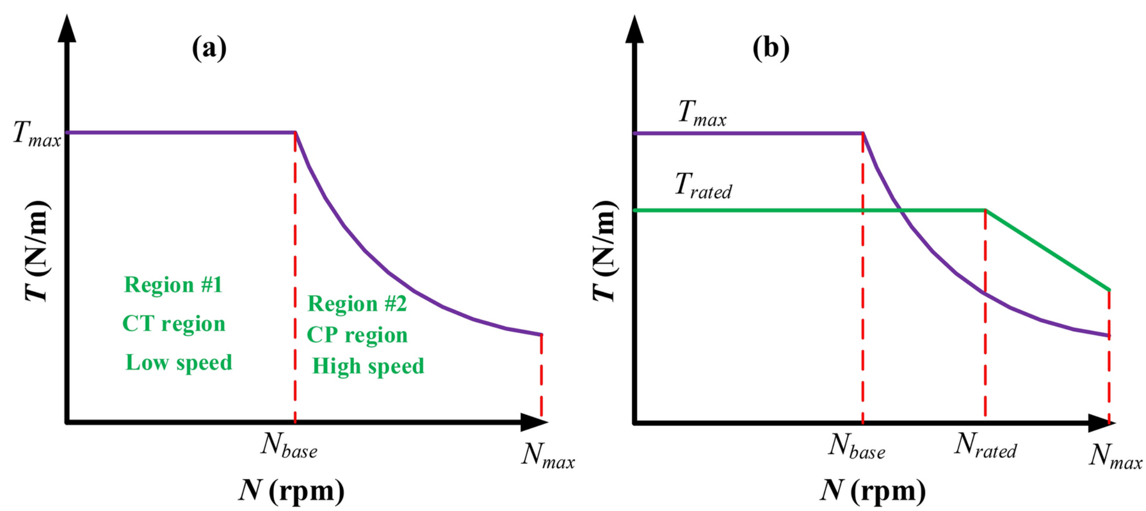

Fig. 1. *T-N* profile for electric motors drives in EVs, (**a**) well-controlled EV motor profile, (**b**) EV motor profile with different α.

- **Unidirectional electric field current technique:** This additional approach is employed to further optimize motor control by ensuring that the current flows in a manner that maximizes efficiency and minimizes losses during motor operation.

By combining these techniques, the proposed control strategy achieves an effective balance between high-performance torque generation, efficient energy use, and operational reliability, making it particularly suitable for EV applications.

The ZDAC technique offers several key advantages for optimizing the performance of electric motor drives in EVs. First, it enables the motor to deliver excellent acceleration from standstill up to the base speed, maintaining the maximum reference torque in the CT region. This reference torque is achieved by controlling the rated stator current, with the q-axis component integrated with the d-axis constant flux, ensuring efficient torque production without saturation. Second, the technique eliminates the reluctance torque inherent in salient pole motors, which also removes the associated harmonics that can negatively impact motor performance. By doing so, it contributes to a smoother and more stable motor operation. Third, the ZDAC approach enhances motor efficiency and improves the overall performance of the inverter. Through precise control of the torque and current, the technique minimizes losses, particularly copper losses, which are a significant source of inefficiency in electric motors. Additionally, the ZDAC method enables a linear torque-current relationship, ensuring optimal torque production at lower energy losses. Finally, one of the main advantages of this technique is its simplicity, which simplifies the control strategy for the motor drive system, making it more robust and easier to implement in practical EV applications.

A unidirectional electric field current plays a crucial role in enhancing the performance of electric motor drives for EVs by supporting the permanent magnet field across the entire operating range of the vehicle. By maintaining a unidirectional field, the technique effectively mitigates the risk of PM demagnetization, which can occur if the magnetic field reverses direction. Reversed flux not only risks demagnetizing the permanent magnets but also introduces significant spatial harmonics that lead to increased core losses, ultimately reducing motor efficiency. The primary objective of the control strategy is to accurately track the reference torque-speed profile of the EV, which includes two distinct operational regions: (i) a high-acceleration region with constant maximum torque, where both stator and field currents are maintained at a constant value to ensure peak performance during low-speed acceleration, and (ii) a wide CP region, where torque is inversely proportional to speed, designed to prevent operation within the motor's natural mode, which could result in instability or inefficiency. Within the CP region, the field current is progressively reduced in a linear fashion as the vehicle speed increases, achieving a smooth transition from the CT region to the constant power region. This gradual reduction of the field current ensures that the motor operates efficiently throughout its speed range. The controller's transition from the CT mode to field weakening mode, which is necessary to maintain high efficiency at higher speeds, is typically determined by the DC bus voltage, indicating when the motor's operating conditions require the shift to avoid exceeding operational limits or compromising efficiency.

ZDAC based steady state mathematical model

The steady-state mathematical model is discussed with and without taking iron core loss into account.

The model with iron core losses effect

Figure 2(a) and (b) show the equivalent circuit of HESM[14,41,42] and the phasor diagram of HESM with ZCAC, neglecting Rc. From this, the ZDAC steady-state mathematical model can be deduced.

The flux linkage with $I_d = 0$ can be written as shown:

$$\lambda_d = \lambda_{pm} + M_{sf} I_f \tag{1}$$

$$\lambda_q = L_q I_q, \tag{2}$$

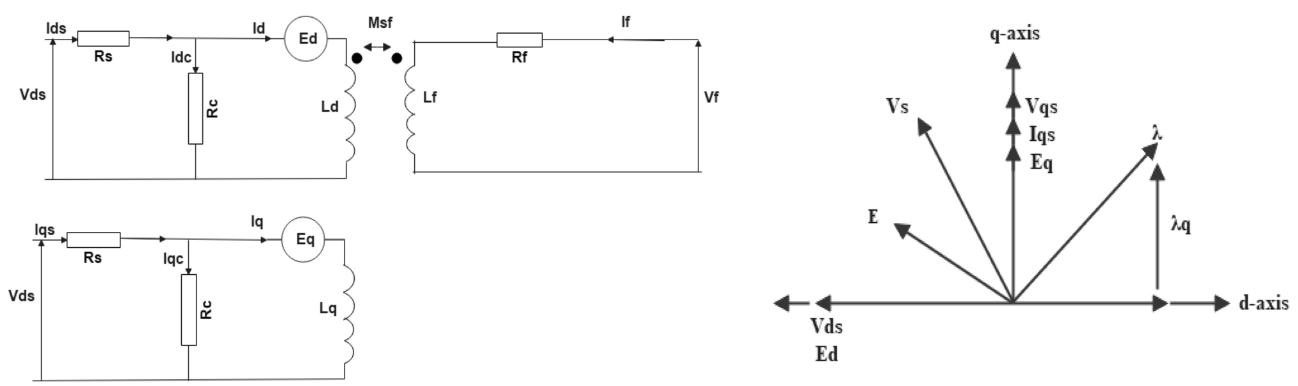

(a) (b)

Fig. 2. (**a**) Equivalent circuit of HESM with ZDC and, (**b**) phasor diagram of HESM with ZDAC with neglected R_c.

So, the stator voltage with ZDAC can be rewritten as follows

$$V_{ds} = R_s I_{ds} + E_d \tag{3}$$

$$V_{qs} = R_s I_{qs} + L_q \frac{d}{dt} I_q + E_q \tag{4}$$

where:

λ_d, λ_q the d- and q-axis flux linkage components,
λ_{pm} the permanent magnet flux linkages,
M_{sf} stator and excitation windings mutual inductance,
V_{ds}, V_{qs} the d- and q-axis stator voltage components.

$$E_d = -\omega_r L_q I_q = -\omega_r \lambda_q \tag{5}$$

$$E_q = \omega_r \left(\lambda_{pm} + M_{sf} I_f\right) = \omega_r \lambda_d \tag{6}$$

$$I_{ds} = I_{dc} = \frac{E_d}{R_c} = \frac{-\omega_r \lambda_q}{R_c} \tag{7}$$

$$I_{qs} = I_q + I_{qc} = I_q + \frac{E_q}{R_c} = I_q + \frac{\omega_r \lambda_d}{R_c} \tag{8}$$

where:

E_d, E_q the d- and q-axis induced EMF components,
I_{ds}, I_{qs} the d- and q-axis stator current components,
I_d, I_q d-q-axis armature inductance current components,
V_{ds}, V_{qs} the d- and q-axis stator voltage components.
So, the stator voltage with ZDAC can be written as follow:

$$\begin{bmatrix} V_{qs} \\ V_{ds} \\ V_f \end{bmatrix} = \begin{bmatrix} R_s + sRL_q & \omega_r M_{sf} R \\ -\omega_r L_q R & 0 \\ 0 & R_f + sRL_f \end{bmatrix} \begin{bmatrix} I_q \\ I_f \end{bmatrix} + \begin{bmatrix} \omega_r \lambda_{pm} R \\ 0 \end{bmatrix} \tag{9}$$

where:

$$R = \frac{R_c + R_s}{R_c} \tag{10}$$

Note that $s = \frac{d}{dt}$ = 0 at steady state operation.

$$V_{ds} = -\omega_r L_q I_q R = -\omega_r \lambda_q R \tag{11}$$

$$V_{qs} = R_s I_q + \omega_r \left(M_{sf} I_f + \lambda_{pm}\right) R = R_s I_q + \omega_r \lambda_d R \tag{12}$$

Electromagnetic torque with ZDC can be given as follow:

$$T = \frac{3}{2} p I_q \left(\lambda_{pm} + \lambda_f\right) \tag{13}$$

This is a sum of PM torque T_{pm} (due to PM excitation) and field torque T_f (due to field excitation), where:

$$\lambda_f = M_{sf} I_f \tag{14}$$

So the total power losses P_l with ZDAC are defined as:

$$P_l = \frac{3}{2} \left[\left({I_{qs}}^2 + {I_{ds}}^2\right) R_s + \left({I_{qc}}^2 + {I_{dc}}^2\right) R_c\right] + {I_f}^2 R_f \tag{15}$$

Accordingly, the required input power increases with decreased efficiency due to stator copper loss increase and the added iron loss given by first and second terms of Eq. (15), respectively. Hence two inequalities constraints must be taken into account for thermal safety and inverter cost as given by Eqs. (16) and (17)

$$\left({I_{qs}}^2 + {I_{ds}}^2\right)/2 \le {I_{a\,max}}^2 \tag{16}$$

$$\left({V_{qs}}^2 + {V_{ds}}^2\right)/2 \le {V_{a\,max}}^2 \tag{17}$$

The power factor angle φ can be given as:

$$\varphi = \left[tan^{-1}(V_{ds}/V_{qs}) - tan^{-1}(I_{ds}/I_{qs})\right] \tag{18}$$

Model without iron core losses effect

The variables that are directly affected by R_c are the d-q flux linkage components λ_d and λ_q each of them is to be scaled by R factor. References[19,40] stated that practically, even at high speeds where core resistance R_c is the lowest, $(R_c/R_s) > 10$, therefore, R tends to one $(R = 1)$. So the stator voltage with ZDC at negligible core resistance can be rewritten as follow:

$$V_{ds} = -\omega_r\lambda_q \tag{19}$$

$$V_{qs} = R_s I_q + \omega_r\lambda_d \tag{20}$$

Also, the d- and q-axis stator current components with ZDAC with negligible core resistance can be rewritten as follow:

$$I_{ds} = I_d = 0 \tag{21}$$

$$I_{qs} = I_q \tag{22}$$

Equation (13) indicates that core resistance has no effect on the developed torque as well as on the output power. But has a significant effect on total power losses So the total power losses P_l with ZDC at negligible core resistance can be rewritten as follow:

$$P_l = \frac{3}{2}{I_q}^2 R_s + {I_f}^2 R_f \tag{23}$$

Proposed EV-MTPT strategy

The EV-MTPT strategy is discussed with and without taking iron core loss into account. The motor control technique must be divided into two operating ranges of CT and CP to track EV profile.

CT-MTPT performance characteristics

The maximum torque or reference torque can be obtained as follows

$$\begin{aligned} &T_m = T_{ref} = \frac{3}{2} p I_{qmax}\left(\lambda_{pm} + \lambda_f\right) \\ &\text{and} \\ &I_{q\,max} = \sqrt{2} I_{ar} \end{aligned} \tag{24}$$

I_{ar} is the rated armature current and λ_f is taken as 30% of λ_{pm} and $I_f = 95\%$ of its rated value (1A). Thus, at the start below and up to base speed, the PM flux strengthening operation is applied by adding constant rated field current.

CP-MTPT performance characteristics

Above base speed, flux weakening control with reduced field excitation voltage using a DC chopper takes place.

The chopper input voltage is obtained from the excitation DC controller (PI). The q reference current control component is proportional with speed inverse to properly trace the load torque. The field current is controlled in continuous linear form as shown in Fig. 3 where:

$$I_f = C_b(N_r - N_{\max}) \tag{25}$$

and C_b is the slop at base speed given by: $C_b = I_{fb}/(N_b - N_{max})$.

Figure 4 illustrates the resulted torque T_{pm}, T_f, and $T_{EV\,opt}$ as explained in section II. The field current control forms the required $T_{EV\,opt}$. Figures 5–15 illustrate comparisons between the HEPMSM characteristics with and without iron losses consideration.

It is obvious that iron loss does not affect torque, thus the output mechanical power is not affected, as well as proven in Fig. 5. However, its effect on input power becomes significant as the speed increases, as shown in Fig. 5 due to its dependency on speed increase.

Figure 6 depicts the armature current and its d-q components with and without iron losses equivalent resistance (R_c) consideration. As shown, the d-axis current is slightly affected by R_c with a low negative value. In contrast, the stator current q-axis component is dramatically increased. Based on this statement, it can be seen that the stator voltage d-q components shown in Fig. 7 are self-explained with almost non-varied d-axis components but with a remarkably increased q-axis one. It's obvious that there will be no effect of the iron losses R_c on the induced air gab back emf created by the two fluxes of the two hybrid excitation sources, as shown in Fig. 8. On the other hand, the stator voltage increases as the speed do over the CP in but within its permissible values.

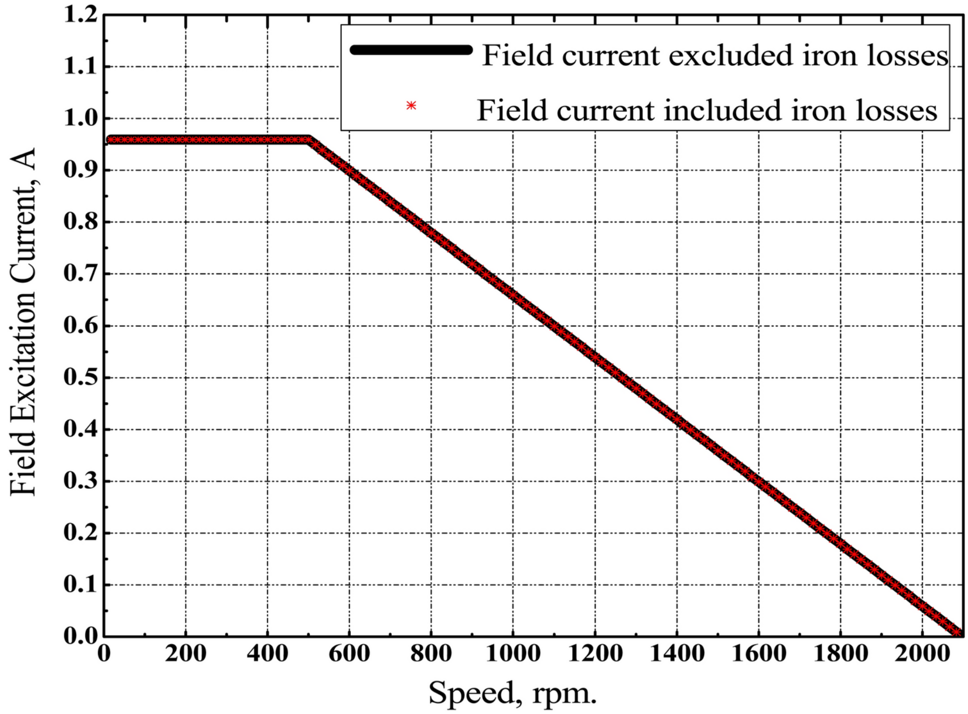

Fig. 3. Field Excitation Current versus speed.

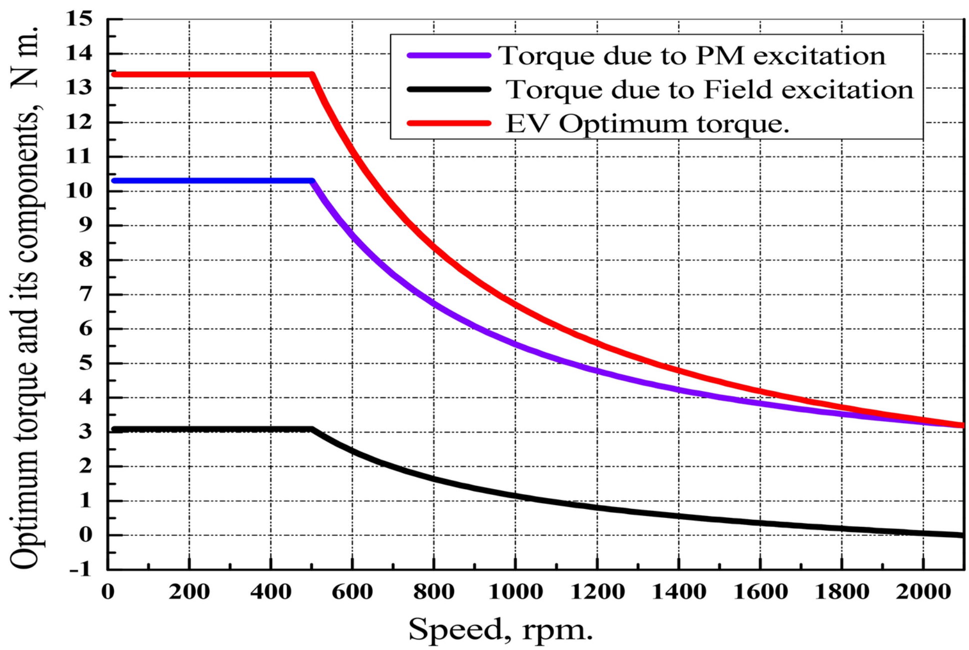

Fig. 4. HEPMSM torque components versus Speed.

The total losses shown in Fig. 9 significantly increase with the speed as expected due to iron losses rapid increase. With ignored iron losses, the total copper losses reach their minimum (armature copper losses) at maximum speed with zero field copper losses.

Figure 10 illustrates the significant high efficiency gained with the proposed control strategy with $Rc \gg Rs$ (iron lossless). The maximum efficiency is addressed at maximum speed. However, high efficiency is gained all over the operating range. The iron losses drag the maximum efficiency towards the middle of the operating speed range, where the iron losses are equal to the total copper losses. The higher the speed, the lower efficiency is.

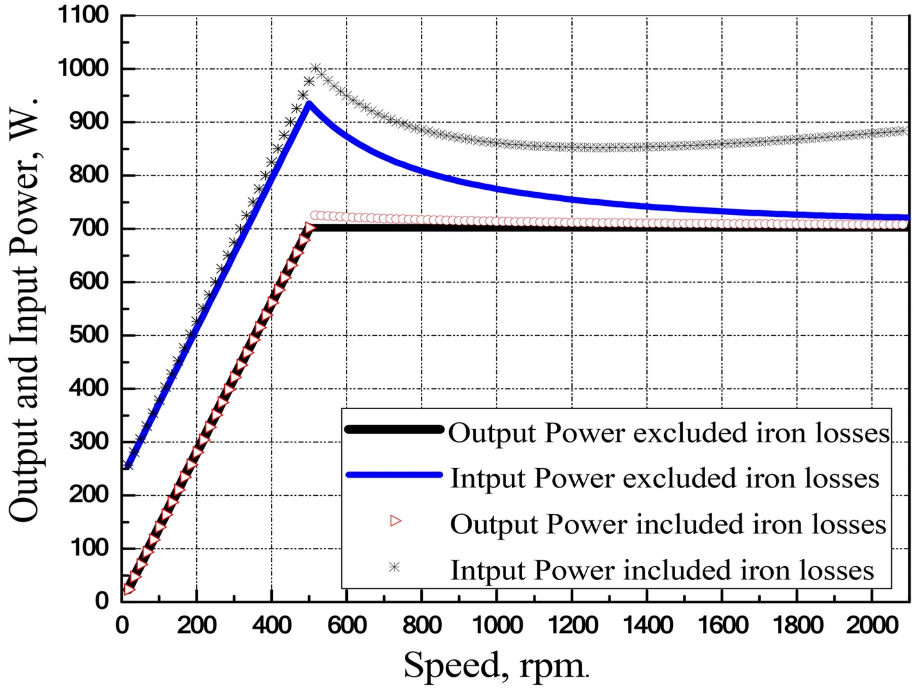

Fig. 5. Output and Input power versus speed.

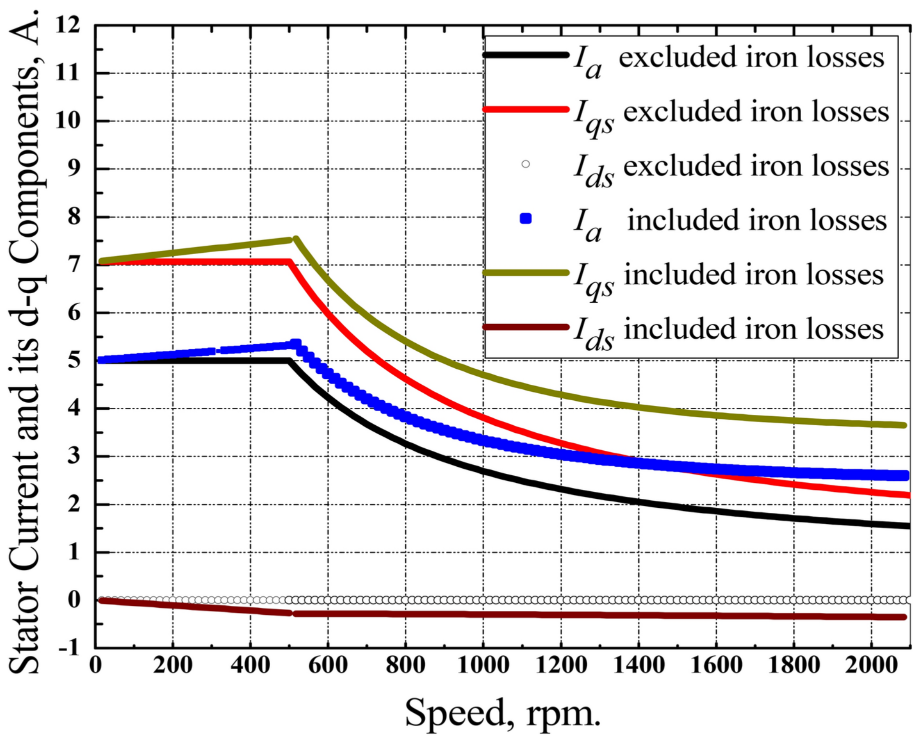

Fig. 6. Stator Current and its d-q components versus speed.

Figure 11 shows that taking R_c into account improves the power factor to be nearer to the unity power factor by a slight increase than that without R_c favourite linear torque- stator current dependency for simple control is introduced over the whole speed range for $R_C \gg R_s$ structure as shown in Fig. 12. With considered R_c, attention must be paid for safe maximum armature current (of 1.1 rated value) if the motor is required to operate at high acceleration. The behavior of the power factor is influenced by several factors tied to motor design and operation across different speed ranges. At low speeds, the motor operates under partial load conditions,

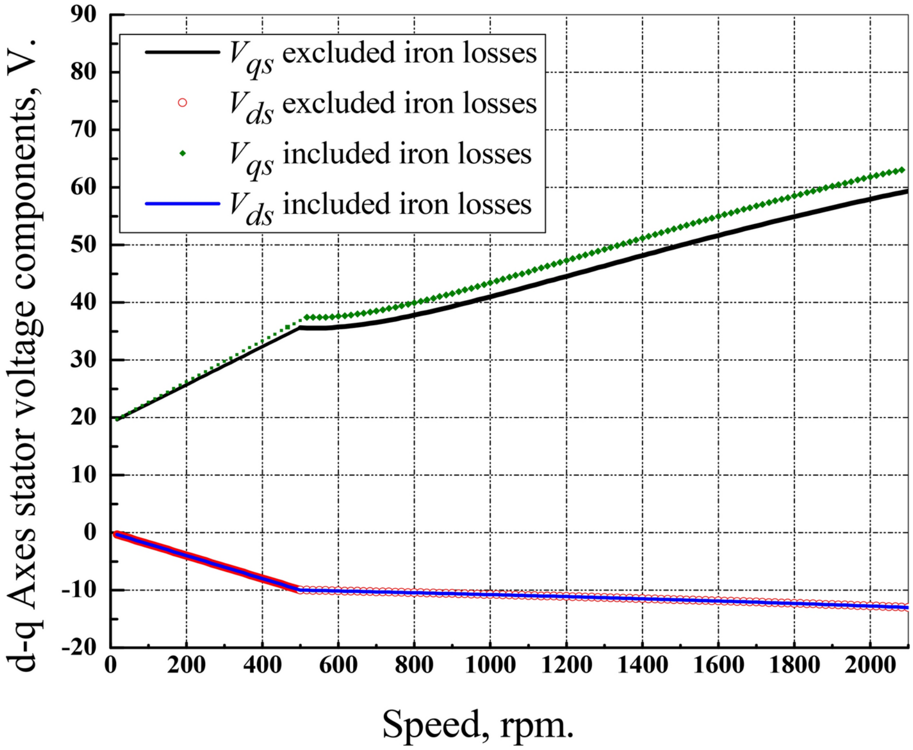

Fig. 7. d-q Stator Voltage Versus Speed.

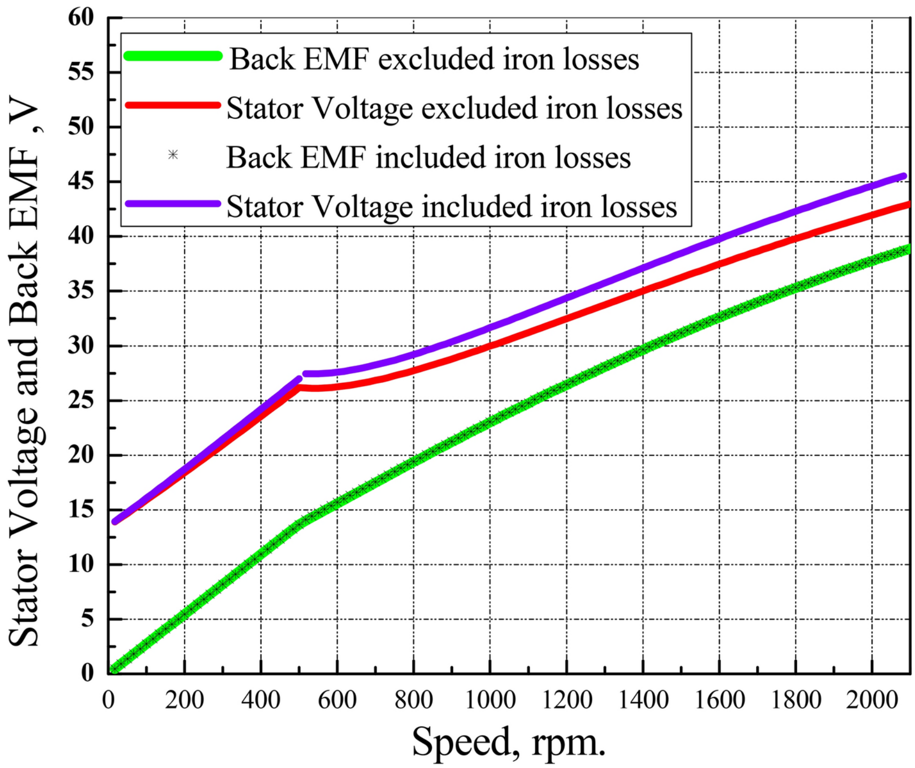

Fig. 8. Stator Voltage and induced emf versus Speed.

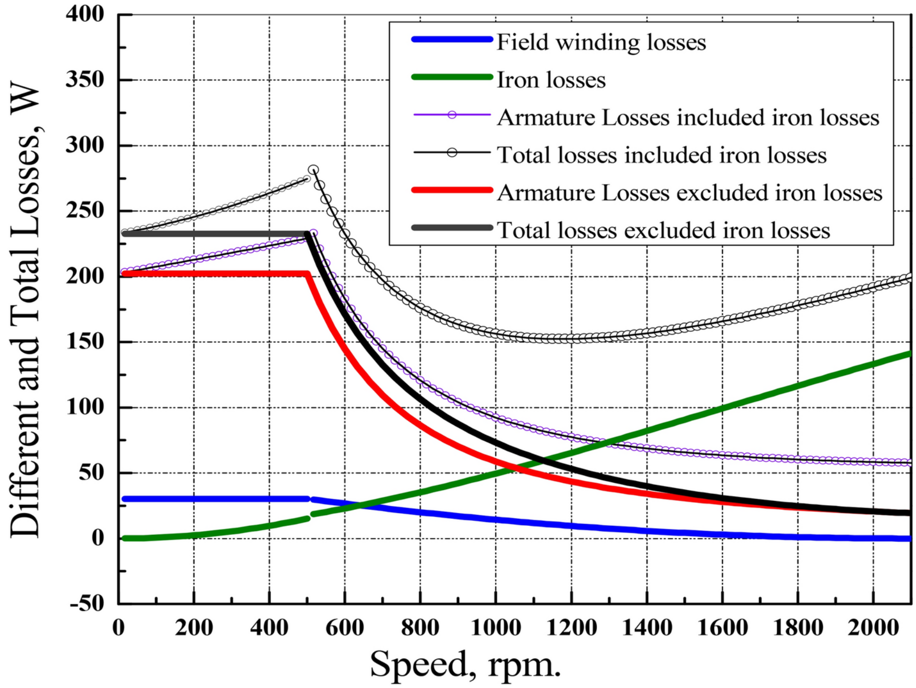

Fig. 9. Different HEPMSM losses versus Speed.

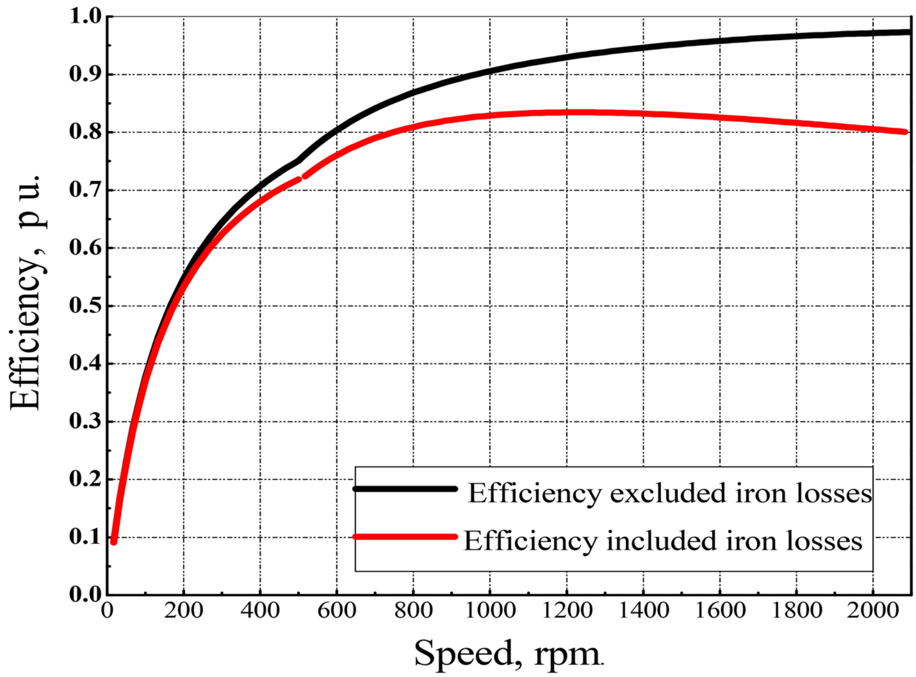

Fig. 10. Efficiency versus Speed.

where the inductive reactance is minimal due to the low operating frequency. However, the presence of iron losses, particularly hysteresis and eddy current losses, increases the apparent power more significantly at lower frequencies, causing the power factor to decrease as the reactive power component, driven by inductance and magnetization, dominates over the real power. As speed increases into the medium range, the operating frequency rises, increasing both inductive reactance and iron losses. The interaction between the excitation flux from the hybrid magnets and the stator flux becomes less optimal, leading to a greater phase difference between voltage and current, resulting in a slight dip in the power factor. At high speeds, the motor's design enables better flux weakening, improving efficiency in managing iron losses and minimizing the dominance

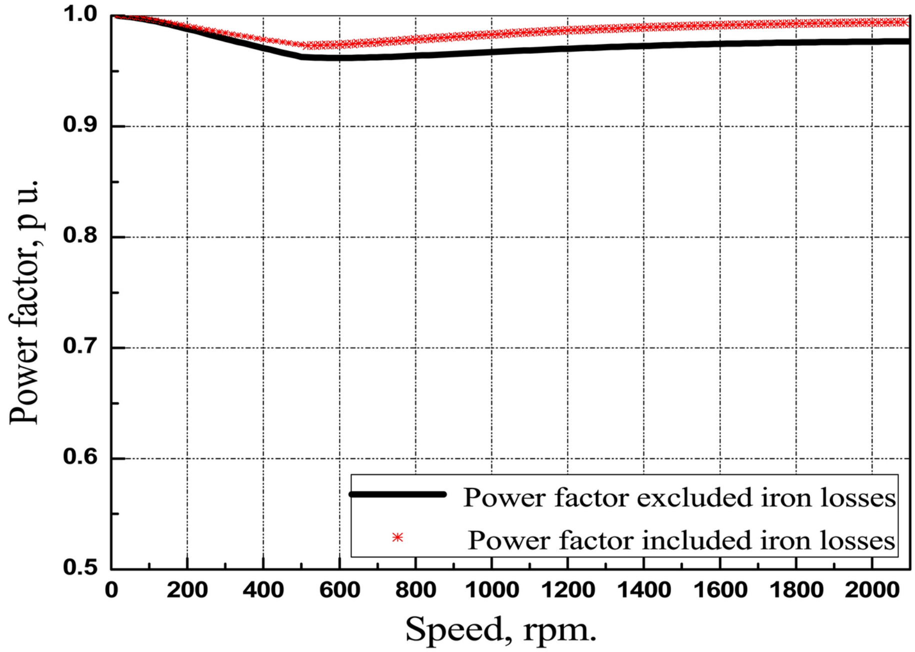

Fig. 11. Power Factor versus Speed.

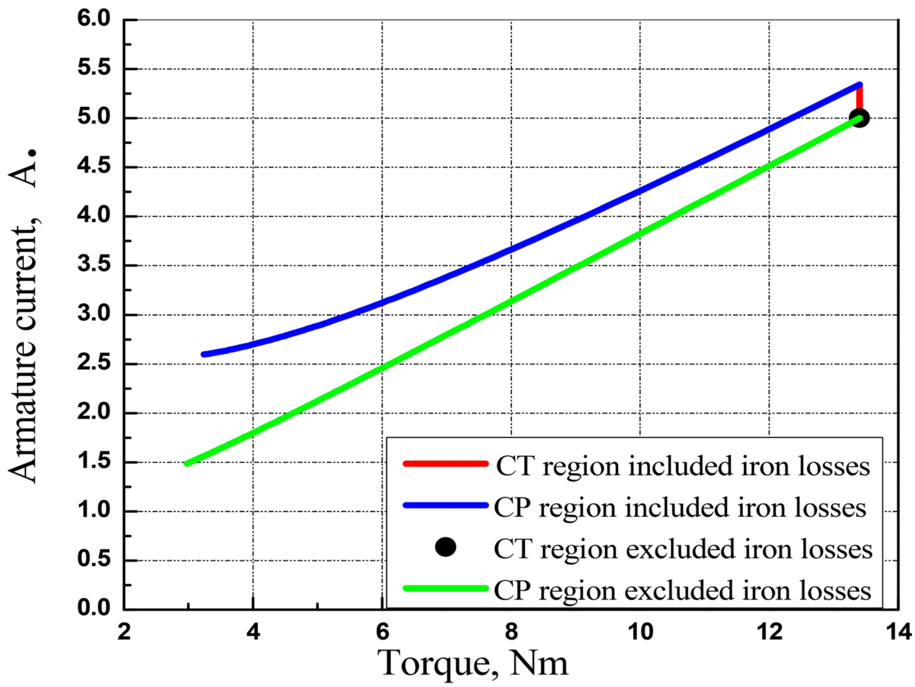

Fig. 12. Stator Current versus Torque.

of inductive reactance. The excitation flux is optimally controlled, reducing the phase lag between voltage and current, which leads to an improved power factor as the reactive power component is minimized. Iron losses throughout the speed range contribute to a lower power factor compared to a scenario without these losses, as they increase the apparent power, thus reducing the ratio of real power to apparent power. In summary, the power factor's variation is a result of the interplay between inductive reactance, flux weakening, and iron losses as the motor transitions through different speed ranges, with reactive effects dominating at low speeds, less optimal flux interaction at medium speeds, and improved power factor at high speeds due to flux weakening and optimized control strategies.

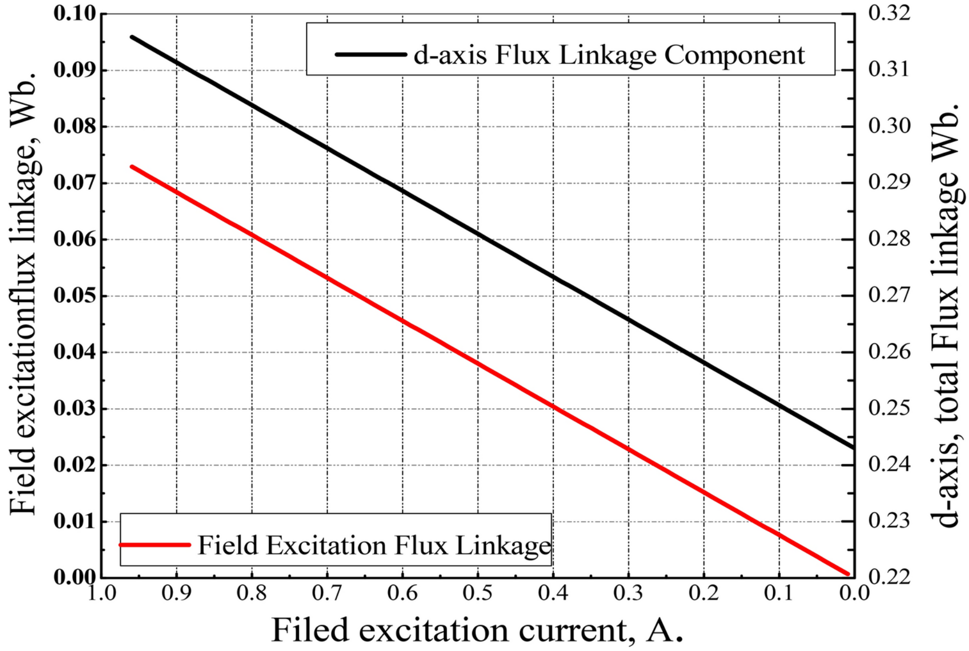

Fig. 13. Field excitation flux linkage and d-axis total flux linkage versus field excitation current.

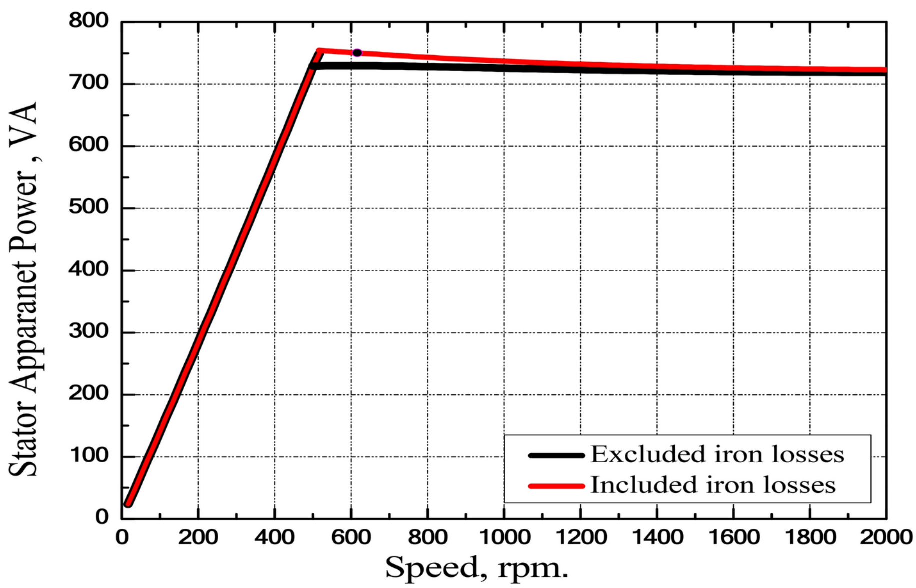

Fig. 14. Stator Apparent Power versus Speed.

Unlike most EV proposed models in the literature, even with a prototype motor[10,24], this paper exhibits a perfect linear relationship between the excitation current and both of the excitation flux linkage and the torque producing flux linkage component, as shown in Fig. 13.

Figure 14 introduces another important target for driving inverter reliability and costs. At low speed, the volt-ampere linearly increases with speed while it is kept constant over the CP region.

EV-MTPT control implementation

In EV drive, torque-based control is more effective than speed-based control as the accelerator varies the torque rather than speed. The computational controller block includes the HEPMSM module, reference currents calculator, and Current Distributor submodule. The current distributor sub-module divides the whole speed-operation range into two regions: the low speed – CT region and high speed -lower torque region, respectively. It regulates the three reference currents $I_f, I_q, and I_d$ thoroughly to be compared with the corresponding measured quantities through the three current controllers as shown in Fig. 15. The q reference current component in the

CP region is based on the reference torque, speed, and field current. Field current gradually decreases as the speed increases in linear mode, achieving a smooth transition between the two CT and CP operating regions. The DC voltage can be varied continuously by changing the duty ratio D, where $1 \geq D \geq 0$. The control process is based on the aforementioned mathematical model. The DC bus voltage may determine when the controller needs to transit into the field weakening mode.

MOALO based performance analysis

A second category based on a search algorithm to define optimum hybridization ratio and base speed is carried out below. In 2017, The authors in[39] developed the MOALO algorithm as a meta-heuristic optimization technique that simulated the hunting mechanism of ant lion predators with their favorite ants in nature. The MOALO begins by generating an ant population, the fitness function, and updating ant and ant lion positions later. It ends by testing the stopping criterion. The general steps describing the MOALO technique are summarized as follows[43]:

1. [Initialization] Generate a random population of ants that move around ant lions in the search space.
2. [Fitness] Evaluate the fitness of each ant position in the space concerning ant lions.
3. [Position Update] Update the position of each ant using random walk concerning the ant lions based on roulette wheel until the best ant lion is obtained and store it as an elite
4. [Evaluation] Evaluate and update the new best ant lion position to their objective values.
5. [Test] If the criterion is achieved, stop and find the current best ant lion position.
6. [Loop] If the number of iterations number equals the maximum stop, else go to step (2) with the best ant lion position obtained in step (5).

MOALO is applied to select the required efficient *HR* and base speed values that optimize the HEPMSM to fit EV. An exhaustive search program is applied without and with iron losses consideration to select both *HR* and N_b at maximum efficiency and widest CP region.

The objective function *F* with inequalities and equalities constraints is given as follows;

(a) objective function; F = max. [η{ HR, N_b,λ_f, K_f }] where K_f is the field current reduction ratio.

(b) Optimization Inequalities:

$$\begin{cases} I_a \leq I_{ar} \\ V_a \leq V_{ar} \\ N_b \leq N_r \\ -\mathrm{I_{fr}} \leq \mathrm{I_f} \leq \mathrm{I_{fr}} \end{cases} \tag{26}$$

(c) Optimization Equalities:

$$\begin{cases} HR = \lambda_f/\lambda_m \\ \lambda_f = I_f M_{sf} \end{cases} \tag{27}$$

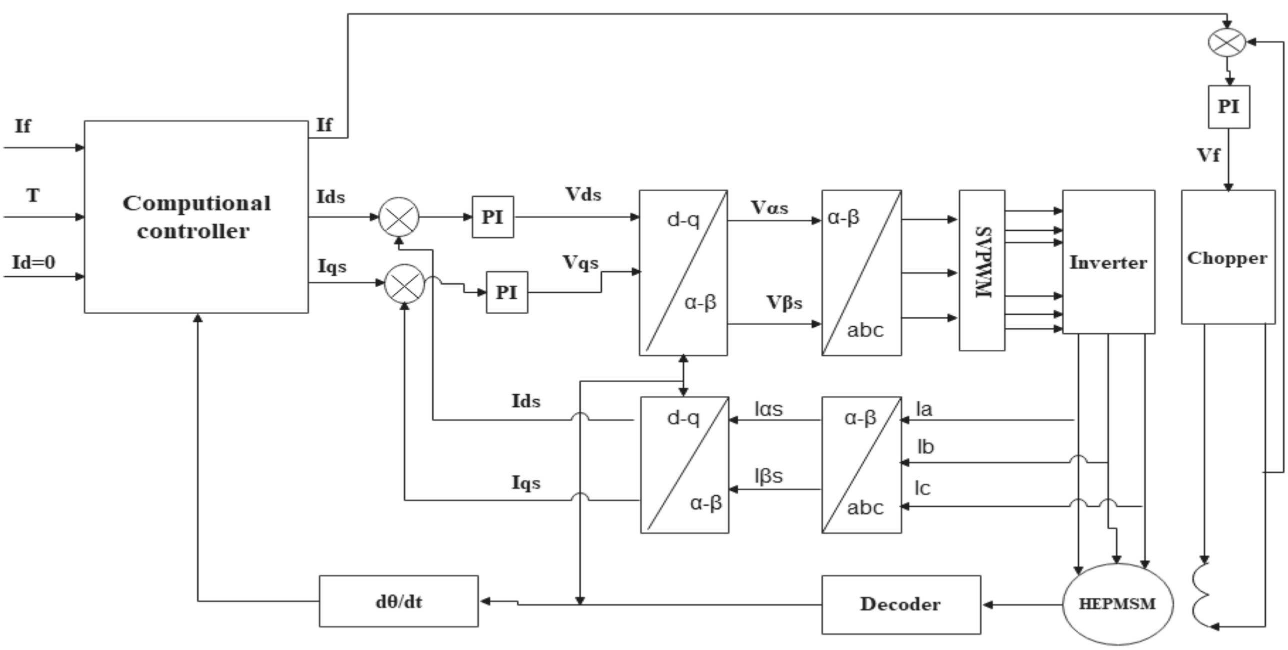

Fig. 15. Proposed Control Strategy of EV HEPMSM.

Parameter	Tb	nb	I_{ar}	I_{fr}	P_r
Value	13	500	5	1	700
Unit	N.m	rpm	A	A	W

Table 1. Motor under study nominal ratings.

	Cases	Case A	Case B	Case C	Case D
	N_b	500	566	625	705
	HR_{CT}	0.3	0.3097	0.289	0.283
Without R_c	$HR_{\eta max}$	0	0.00938	0.022	0.037
	η_{max}	96.95	96.77	96.41	95. 23
	$N_{\eta max}$	2100	2100	2100	2100
With R_c	$HR_{\eta max}$	0.14	0.147	0.15	0.15
	η_{max}	81.59	83.56	82.38	82.58
	$N_{\eta max}$	1290	1335	1380	1455
	$\eta_{N max}$	81.39	81.36	80.61	79.93
	P_o	700	794	877	990

Table 2. Comparison between MOALO results with and without iron losses consideration.

The search program is applied without and with iron losses to be compared with the proposed numerical category. The searching algorithm has more freedom for reversing field current, varying HR, and base speed to select an optimum combination. Otherwise same control basics given in the modelling strategy are applied.

Optimization results and discussions

MOALO obtained optimized results at variable HR and N_b without and with iron losses consideration are illustrated in Table 1 and Table 2. As stated in Section II, the optimization control strategy exhibits advantages of low-speed high-torque, wide CP range, and high efficiency in the flux-weakening (CP) region. With EV-HEPMSM, the design of base speed and efficiency maximization is an immediate obligation. Under the constraints used here, the efficiency and base speed were optimized simultaneously as Mir Jalili functions using MOALO. The resulted values in accordance with η_{max} and N_b. 10,000 iterations for every loop were examined by the search algorithm to reach the final optimum values A, B, C, and D. Case A represents the non-dominated solution within the motor ratings of current, voltage, and output power. Case B, C, and D represent a slightly higher efficiency, but the main problem is the overrated values of output power. It's clear that as listed in Table 1. Case A satisfies all the system requirements optimally. Cases B, C, and D represent non-optimal cases as each of them violates the over-design problem regardless of an iron loss considering or not. It is worth noting that with Rc consideration, the searched maximum efficiency magnitude and position are significantly decreased where the hybridization ratio is much higher than that with neglected R_c.

From the above-given Table 2, the following main notes are to be considered:

1- For maximum torque production over the CT region, there is a great integration and dependency between the torque the armature current I_a and field current I_f with varied HR. Apart from the unique optimum values (5, 0.954), any reduction of each brings the other over-designed.
2- Stator voltage's q-d components are slightly affected by HR variation.
3- The higher the positive CT-HR (unidirectional field current), the higher the efficiency is. However, care must be paid to avoid thermal and over-designed problems.

MOALO optimized performance characteristics

The obtained MOALO optimization results given in Table1 are used to illustrate the complete optimized performance characteristics of EV-HEPMSM over the operating speed range. The derived characteristics of Figs. 15(a-d) and 16(a-d) present the four cases of A, B, C, and D with and without R_c for quantifying each state. For an easy comparison, the figures are illustrated so that the comparison validity between the A case performance characteristics with its corresponding ones resulted from the proposed mathematical model given in Sect. "Optimization Results and Discussions". Further, Fig. 16 (a-e) illustrate the impact of HR Variation on the torque–current control components I_f, I_a, *PF*, and total copper losses.

In general, increasing HR ratio has no effect on the accelerating torque, however, it increases base speed while decreases CP speed range as well as increased accelerating time, stator current, total losses and relatively small efficiency decrease where maximum efficiency is reached at minimum copper losses and maximum speed in iron lossless motor. With an iron lossless system, all aforementioned variables are within their limited values. On the other hand, iron losses significantly affect the efficiency map (magnitude and position) where the resulted maximum efficiency occurs approximately near the middle of the CP speed range (at total minimum losses). The dramatical efficiency reduction is not only due to iron losses but also to increased field losses (at high HR)

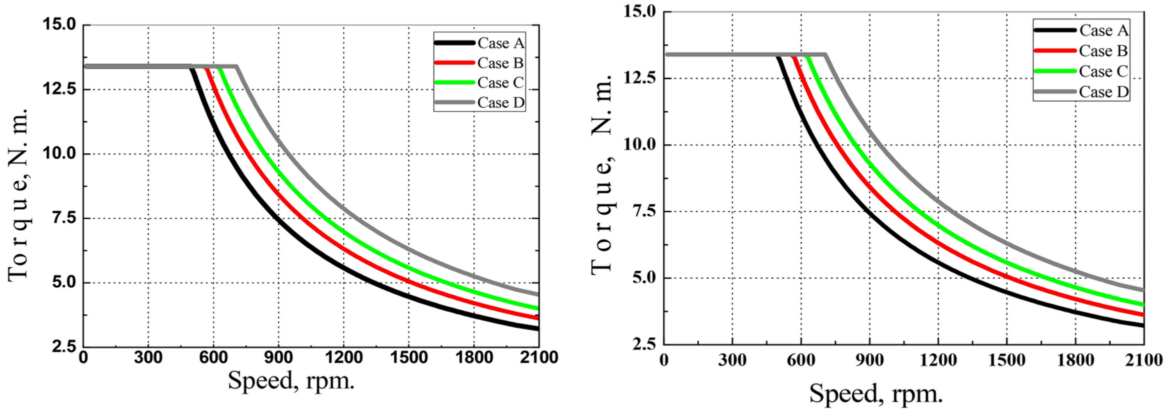

Neglected R_c With R_c

a) Optimized torque versus speed

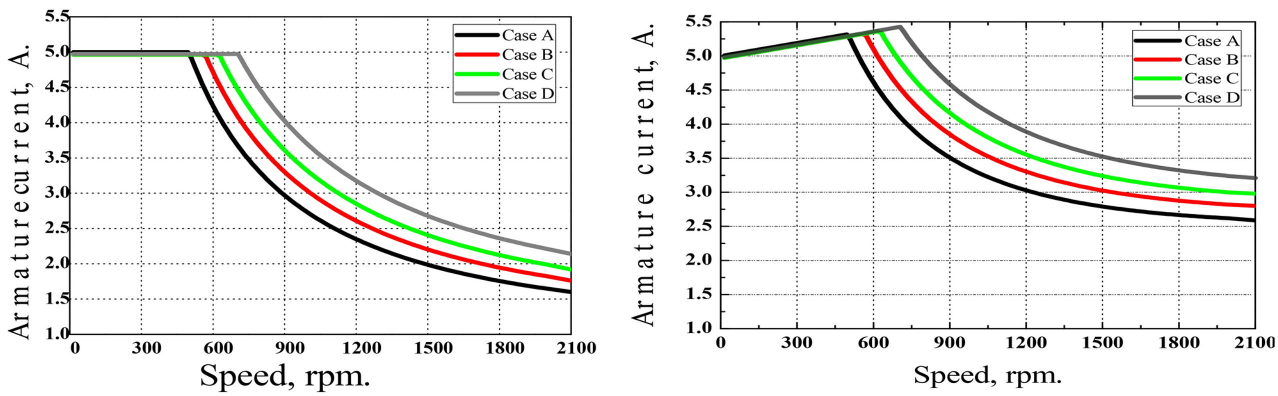

Neglected R_c With R_c

b) Optimized armature current versus speed

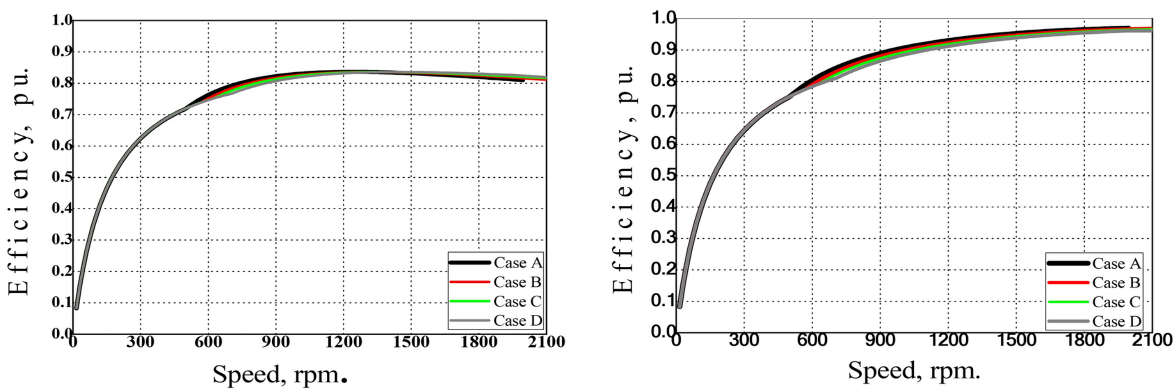

Neglected R_c With R_c

c) Optimized efficiency versus speed

Fig. 16. MOALO obtained compared characteristics with neglected R_c and non-neglected R_c.

and armature copper losses. Thermal consideration must be taken when considering iron losses. From the above results, CT region is the one having the highest stator and field current. Thus, optimized HR must be considered for the thermal state, high acceleration and over design problems. For more evident presentation, the effect of HR with one more allowable reversing freedom on the machine parameters but at the non-dominated constant base speed, constant rated mechanical power, and neglected Rc is carried out as given in Table 3.

It can be concluded with the aid of Fig. 17(**a-d**) that the optimizer results validate the 500 rpm with 0.3 HR as the optimum values for the presented HEPMSM.

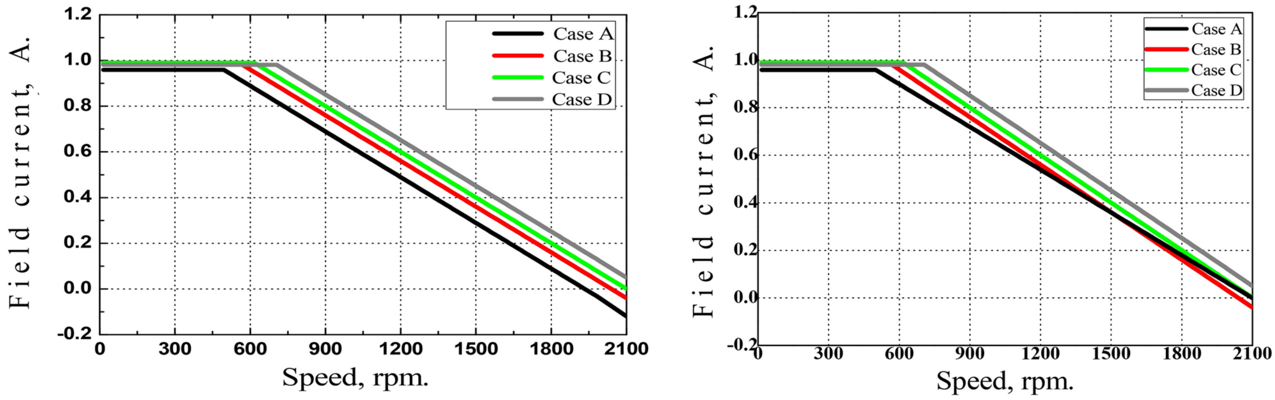

Neglected R_c With R_c

d) Optimized field current versus speed

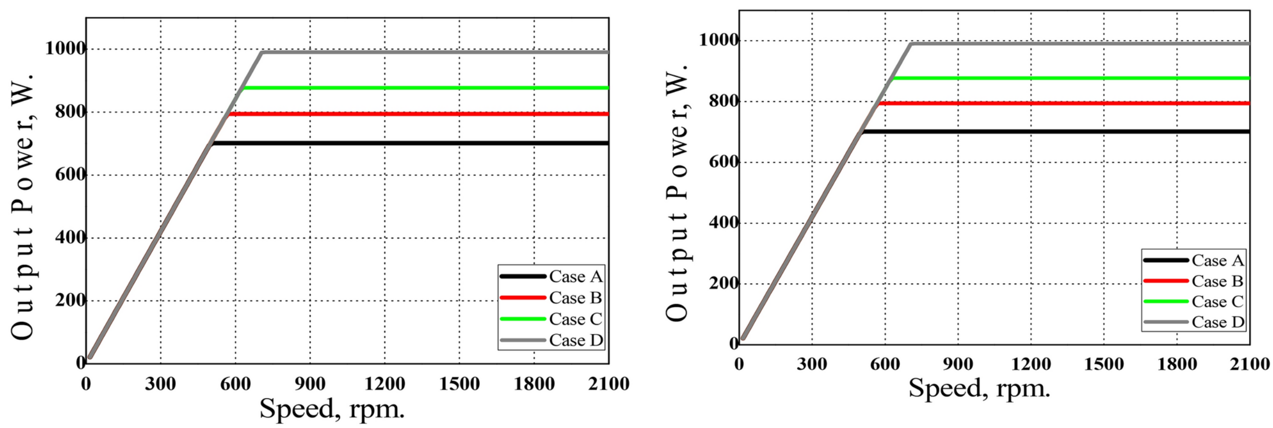

Neglected R_c With R_c

e) Optimized output power versus speed.

Figure 16. (continued)

N_b	500	500	500	500	500
$HRatCT$	0.20	0.25	0.30	0.35	0.40
$I_a atN_b$	5.43	5.19	5	4.78	4.66
$I_f atN_b$	0.64	0.80	0.954	1.10	1.28
$V_{qs} atN_b$	35.6	35.54	35.54	35.6	35.7
$V_{ds} atN_b$	–11	–10.9	–10	–9.7	–12.3
$HR_{\eta max}$	–0.13	–0.084	0	0.015	0.06
η_{max}	95.63	96.48	96.95	97.37	97.42

Table 3. Optimization results for selecting optimum ratio at Constant base Speed Nb.

Simulation modeling and results

Simulations are carried out according to the MTPT, and minimum copper losses control system model explained in Sect. "CT-MTPT Performance Characteristics". and Sect. "ZDAC Based Steady State Mathematical Model" but with $s = d/dt$. The simulation analysis is performed in detail over CT and CP using MATLAB /Simulink model of iron lossless HEPMSM as shown in Fig. 18(a). The motor block diagram contains blocks of d-axis, q-axis, field winding, and Torque components. Torque maximization block implements the MTPT technique at the CT region by maximizing I_q and I_f values. Efficiency maximization block implements ZDAC in both CT and CP regions, which eliminated total motor copper losses. Condition selector block enables the controller to select between CT and CP region by measuring the motor speed then applying the suitable algorithm. The torque block was built to fit the proposed control strategy of efficiently tracking the torque-speed envelope of EV over

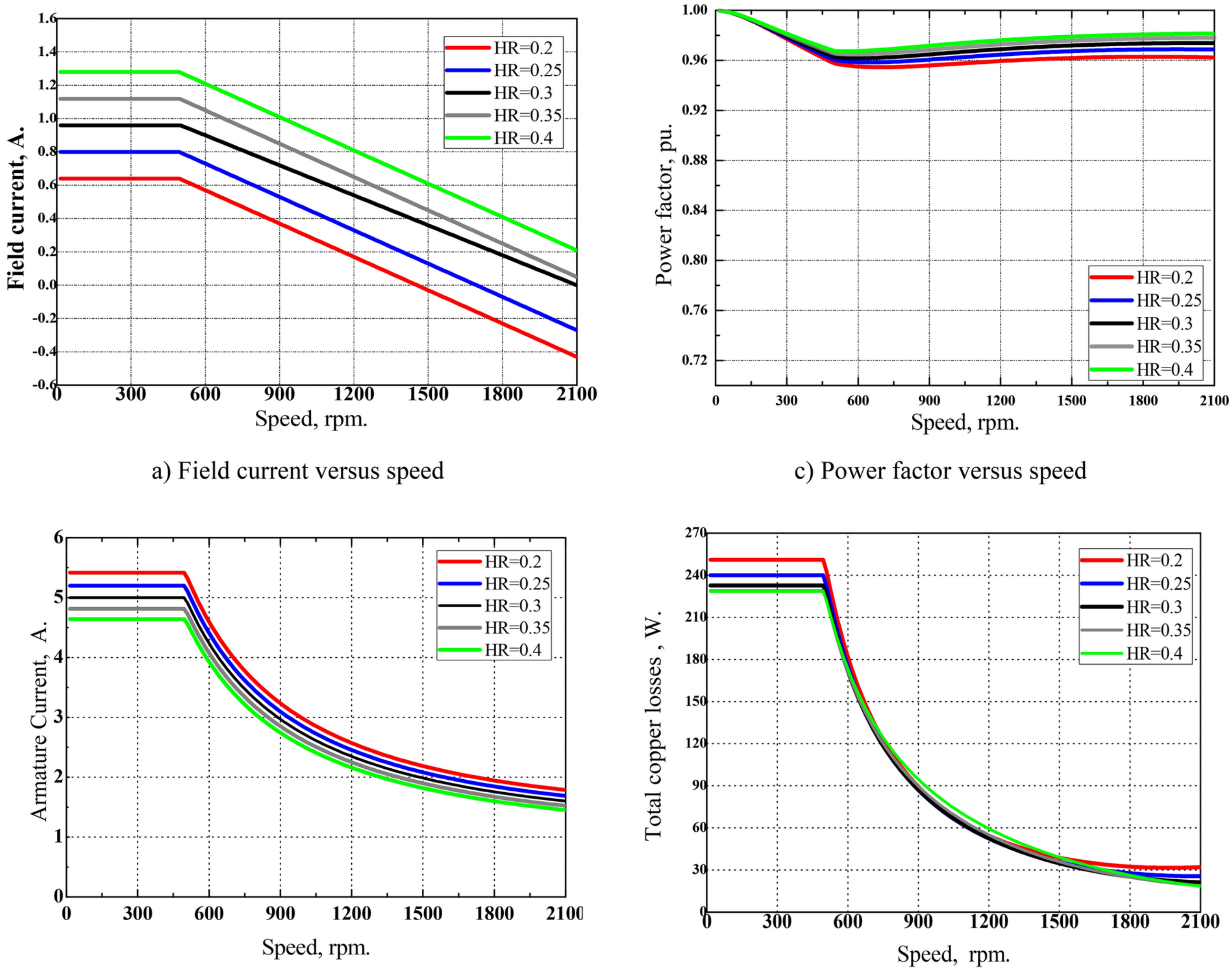

a) Field current versus speed

c) Power factor versus speed

b) Armature current

d) Total copper losses versus speed

Fig. 17. Different HR at constant base speed.

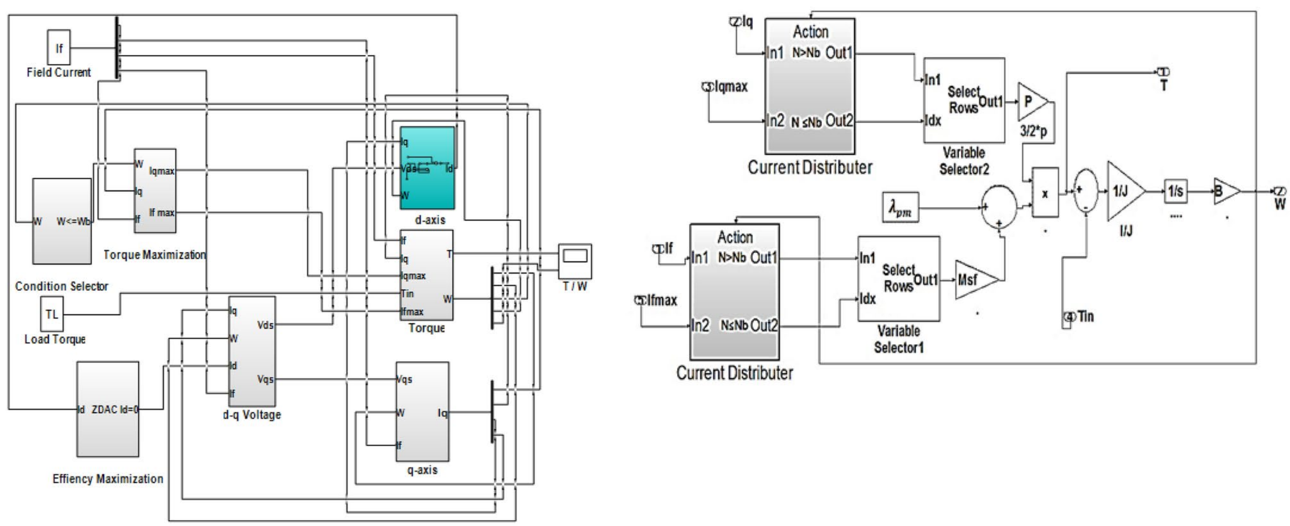

a)

b)

Fig. 18. (**a**) HEPMSM Simulation block diagram, (**b**) HEPMSM torque component block diagram.

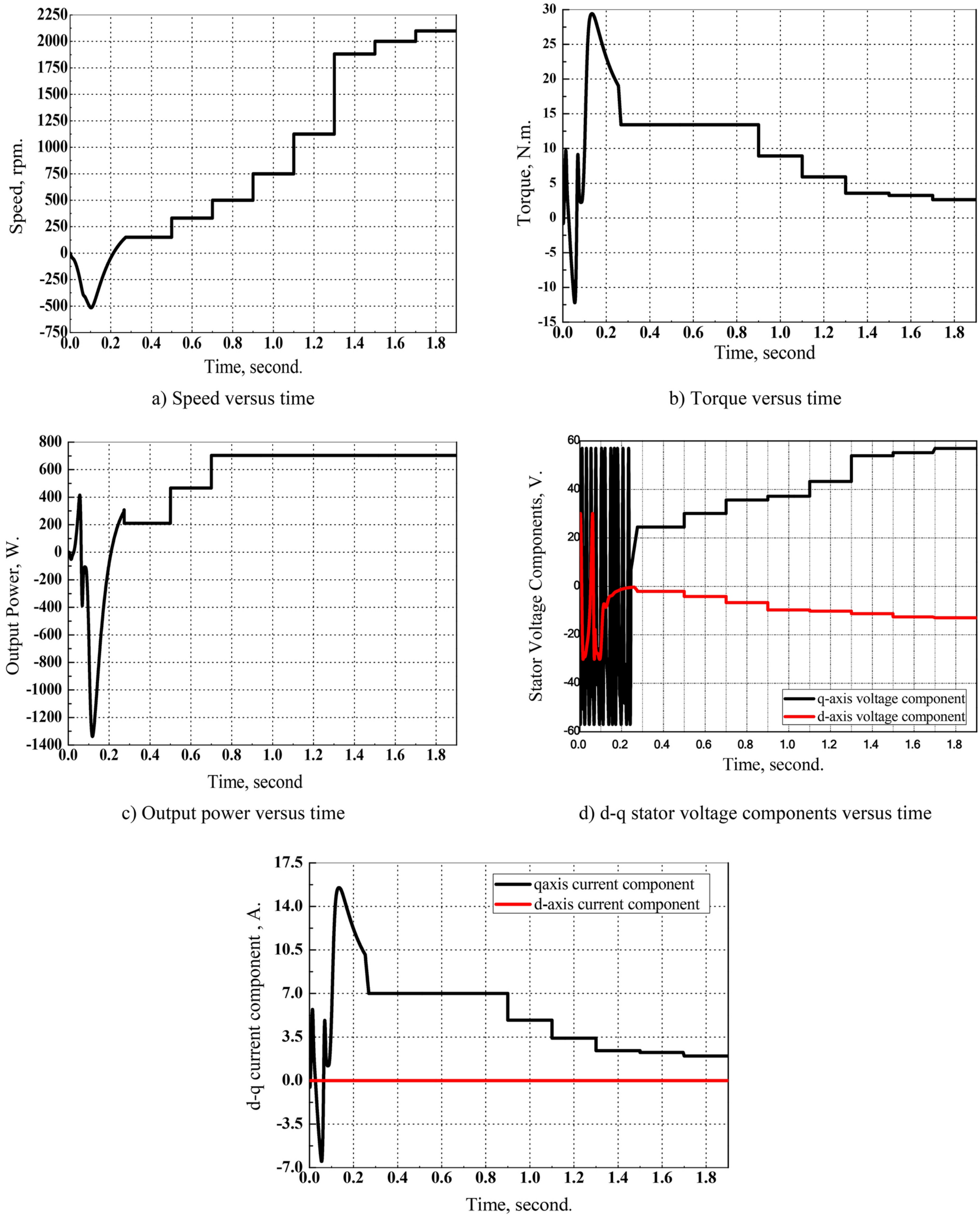

a) Speed versus time

b) Torque versus time

c) Output power versus time

d) d-q stator voltage components versus time

e) Speed versus time

Fig. 19. Simulation results of the dynamic operation of HEPMSG comparing with steady-state operation.

the whole operating speed range using two current distributors, as shown in Fig. 18(b). Figure 19 depicts the simulated performances in two groups, where the first group of Figs. 19(a-f) depicts the motor characteristics' dynamic behavior indicating a smooth transition from CT into CP region and fast acceleration up to cruise speed with an ideal small time. On the other hand, the MATLAB simulation is further based on MOALO results. Figures 19(f,g, and h) depict torque, d-q stator voltage components, and output power, respectively from which both dynamic and steady-state characteristics coincide with each other.

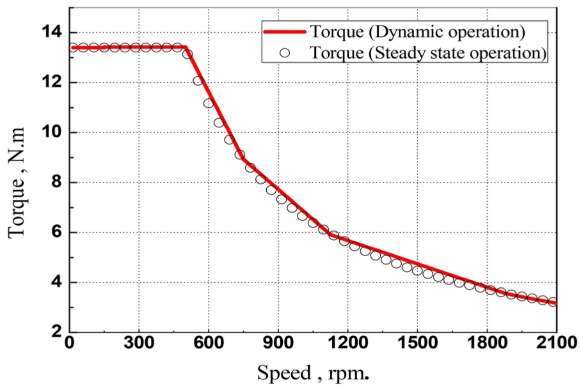

f) Torque versus speed

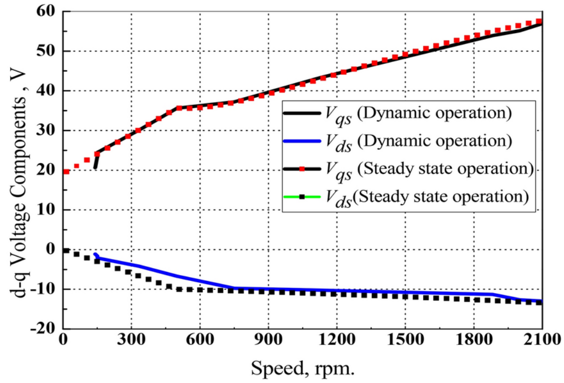

g) d-q stator voltage components versus speed

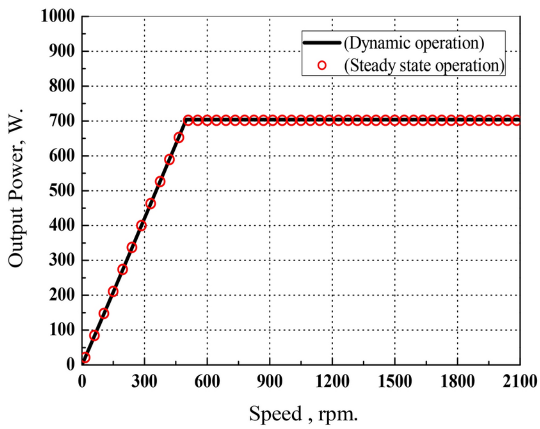

h) Output power versus speed

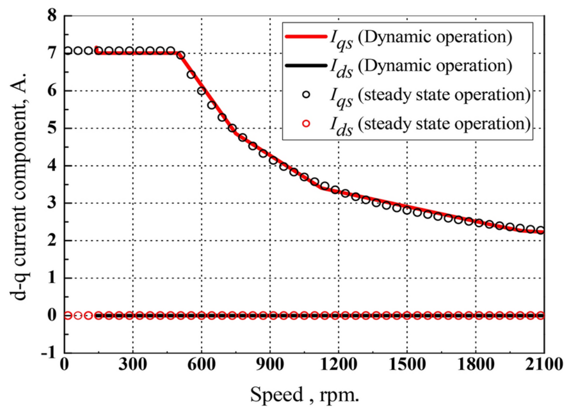

i) d-q stator current components versus speed

Figure 19. (continued)

Figure 19(a) shows that the motoring speed starts getting stable at 0.22 s due to motor inertia. The transition from CT to CP occurred at 0.68 s, proving the high acceleration proposed by the applied control strategy. The motor reaches its maximum speed of 2096 at 1.9 s, which is considered a short time that would be preferred by EV manufacturing. Consequently, Figs. 19(b and c) showed the dynamic torque and output power of the motor, which indicates that the steady CT region starts at 0.26 s and lasts for 0.68 s to steadily continue with the CP region until it reaches maximum speed and minimum torque of 2.67 N.m at 1.9 s.

Figure 19(d) shows the dynamic changes in d-q voltage components due to the acceleration of the motor from CT to CP till the maximum speed at Vq = 58.7 V. It's noticeable that voltage components increase gradually with increased speed, proving another effectiveness of the proposed control algorithm.

The q axis current component starts getting stable at 0.26 s in the CT region with the maximum value of 6.98 A till its minimum value of 2.09 A at maximum speed while the d axis current is kept at zero value due to ZDAC. It's observable from Figs. 19(b and e) the linear relationship between torque and stator current which provides the advantages of fast response and stabilized control.

Torque current component I_q is stepped with the torque, whereas flux current component I_d has zero value as shown in Fig. 19(i). The results obtained based on the suggested base speed, and hybridization ratio are highly validated by the Matlab simulated results as shown in the figures. Figures 19(f,g,h) depict torque, d-q stator voltage components, and output power, respectively from which both dynamic and steady-state characteristics coincide with each other with a non-remarkable per cent error of less than 1% . It can be noticed that good agreement between both dynamic and steady-state characteristics over the whole operating range apart from the d- axis voltage dynamic characteristic of the figure as it deviates a bit towards rated speed over the CT region with an acceptable per cent error of 1.89%. This may be referred to $L_d \frac{di_d}{dt}$ and $L_f \frac{di_f}{dt}$ effect.

Conclusion and future works

The proposed control strategy introduces a coordinated operation between the field current and stator q-axis current control, precisely tuned to track the ideal EV torque-speed profile. The primary objectives of this study are maximizing efficiency and extending the constant power (CP) operating region. The impacts of main parameters, including base speed (N_b), hybridization ratio (HR), and iron losses, were comprehensively analyzed using a prescribed mathematical model. The results reveal that when iron loss equivalent resistance is accounted for, a higher HR is required, which significantly reduces the constant power speed ratio (CPSR) and diminishes both the magnitude and position of peak efficiency. The base speed, constrained to satisfy $N_b < N_{rated}$, is complemented by a linear and unidirectional reduction of HR across the CP speed range. To achieve optimal performance while avoiding over-design issues, the MOALO algorithm was employed in a two-step optimization process. The first step involved selecting optimal N_b and HR values, ensuring the system remains within design limits across variable conditions. The second step optimized HR to maximize efficiency under fixed base speed and rated output power constraints. The optimization results demonstrate that the proposed strategy successfully aligns with the practical torque-speed profile and operational requirements of EVs. The strong agreement between the steady-state characteristics derived from the mathematical model and MOALO-optimized results validates the approach. MATLAB/Simulink simulations further substantiated the effectiveness of the control strategy. For systems without iron losses, all critical variables remained within permissible limits, confirming high efficiency and reliability. However, the inclusion of iron losses introduced a notable reduction in the efficiency map, with the maximum efficiency occurring near the midpoint of the CP speed range, where total losses are minimized. This efficiency reduction stems not only from iron losses but also from increased field and armature copper losses at elevated HR levels. These findings underscore the importance of advanced thermal management and material optimization to mitigate the detrimental effects of iron losses and sustain high performance under real-world conditions. Building on the achievements of this work, the following directions can be anticipated for future research:

- Develop robust cooling systems for HEPMSMs to address the thermal effects of iron losses and improve operational reliability at high speeds.
- Investigate alternative materials for reducing dependency on rare earth elements and improving magnet durability under extreme operational conditions.
- Incorporate other bio-inspired optimization methods, such as Particle Swarm Optimization (PSO), to further enhance the dynamic performance and reliability of HEPMSMs.
- Construct physical prototypes of the proposed motor to validate the findings experimentally and analyze long-term operational stability.
- Explore the integration of HEPMSMs with renewable energy-powered EV chargers, enabling more sustainable powertrain systems.
- Conduct field trials under varying road conditions and loads to evaluate the scalability of the proposed control strategy in commercial EV applications.

Data availability
The data used to support the findings of this study are available from the corresponding author upon request.

Received: 5 December 2024; Accepted: 27 February 2025
Published online: 05 March 2025

References
1. de Santiago, J. et al. Electrical motor drivelines in commercial all-electric vehicles: A review. *IEEE Trans. Veh. Technol.* **61**(2), 475–484. https://doi.org/10.1109/TVT.2011.2177873 (2012).
2. Mom, G. *The electric vehicle: Technology and expectations in the automobile age* (JHU Press, 2013).
3. *Electric and hybrid vehicles : Design fundamentals*. CRC Press 2021 https://doi.org/10.1201/9780429490927
4. Un-Noor, F., Padmanaban, S., Mihet-Popa, L., Mollah, M. N. & Hossain, E. A comprehensive study of key electric vehicle (EV) components, technologies, challenges, impacts, and future direction of development. *Energies* **10**, 8. https://doi.org/10.3390/en10081217 (2017).
5. M. Kebriaei, A. H. Niasar, & B. Asaei, Hybrid electric vehicles: An overview In *2015 International Conference on Connected Vehicles and Expo (ICCVE)* 299–305 https://doi.org/10.1109/ICCVE.2015.84. (2015)
6. A. M. Lulhe & T. N. Date, A technology review paper for drives used in electrical vehicle (EV) & hybrid electrical vehicles (HEV) In *2015 International Conference on Control, Instrumentation, Communication and Computational Technologies (ICCICCT)* 632–636 https://doi.org/10.1109/ICCICCT.2015.7475355(2015)
7. A. Loganayaki & R. B. Kumar, Permanent magnet synchronous motor for electric vehicle applications In *2019 5th International Conference on Advanced Computing & Communication Systems (ICACCS)* 1064–1069 https://doi.org/10.1109/ICACCS.2019.8728442 (2019)
8. Nadia, E. A., Mohamed, E. A. & Mahmoud, E. Assessment of proposed maximum power point tracking–unity power factor algorithms for optimum operation permanent magnet synchronous generator–based wind turbine. *Wind Eng.* **45**(2), 381–399. https://doi.org/10.1177/0309524X20901624 (2021).
9. Gang, Z. & Wang, H. J. Comparison of control methods of permanent magnet synchronous motor in electric vehicle. *Appl. Mech. Mater.* **556–562**, 1396–1399. https://doi.org/10.4028/www.scientific.net/AMM.556-562.1396 (2014).
10. Zhang, F. et al. A new on-board charging-driving integrated topology for V2G technology. *World Electr. Veh. J.* **12**, 4. https://doi.org/10.3390/wevj12040231 (2021).
11. Lu, R., Liu, Z., Liu, X., Sun, B. & Liang, J. "Investigation of a novel intensifying-flux hybrid excited permanent magnet machine for electric vehicles", *COMPEL. Int J. Comput. Math. Electr. Electron. Eng.* **43**(5), 993–1006. https://doi.org/10.1108/COMPEL-11-2023-0572 (2024).
12. Elymany, M. M., Enany, M. A. & Elsonbaty, N. A. Hybrid optimized-ANFIS based MPPT for hybrid microgrid using zebra optimization algorithm and artificial gorilla troops optimizer. *Energy Convers. Manag.* **299**, 117809. https://doi.org/10.1016/j.enconman.2023.117809 (2024).
13. M. Hendijanizadeh, S. M. Sharkh, & A. A. Qazalbash, Comparison of PM and hybrid excited machines for marine vessel hybrid-electric propulsion In *2018 XIII International Conference on Electrical Machines (ICEM)* 602–608. https://doi.org/10.1109/ICELMACH.2018.8507207(2018)
14. Elsonbaty, N. A., Enany, M. A. & Hassanin, M. I. An efficient vector control policy for EV-hybrid excited permanent-magnet synchronous motor. *World Electr. Vehicle J.* **11**(2), 42. https://doi.org/10.3390/wevj11020042 (2020).
15. Zhu, Z. Q. & Cai, S. Hybrid excited permanent magnet machines for electric and hybrid electric vehicles. *CES Trans. Electr. Mach. Syst.* **3**(3), 233–247. https://doi.org/10.30941/CESTEMS.2019.00032 (2019).

16. Wang, Y. & Deng, Z. Hybrid excitation topologies and control strategies of stator permanent magnet machines for DC power system. *IEEE Trans. Ind. Electron.* **59**(12), 4601–4616. https://doi.org/10.1109/TIE.2012.2183842 (2012).
17. Mingming, H. et al. Flux-weakening control methods for hybrid excitation synchronous motor. *Arch. Electr. Eng.* **64**(3), 427–439 (2015).
18. Kupiec, E. & Przyborowski, W. Magnetic equivalent circuit model for unipolar hybrid excitation synchronous machine. *Arch. Electr. Eng.* **64**(1), 107–117 (2015).
19. Zhang, Z., Liu, Y., Tian, B. & Wang, W. Investigation and implementation of a new hybrid excitation synchronous machine drive system. *IET Electr. Power Appl.* **11**(4), 487–494. https://doi.org/10.1049/iet-epa.2016.0542 (2017).
20. Asfirane, S., Hlioui, S., Amara, Y. & Gabsi, M. Study of a hybrid excitation synchronous machine: modeling and experimental validation. *Math. & Comput. Appl.* **24**(2), 34. https://doi.org/10.3390/mca24020034 (2019).
21. O. Wallmark, On control of permanent-magnet synchronous motors in hybrid-electric vehicle applications 2004
22. Paplicki, P. A novel rotor design for a hybrid excited synchronous machine. *Arch. Electr. Eng.* **66**(1), 29–40 (2017).
23. Xu, G., Liu, G., Du, X. & Bian, F. A novel PM motor with hybrid PM excitation and asymmetric rotor structure for high torque performance. *AIP Adv.* **7**(5), 056671. https://doi.org/10.1063/1.4978400 (2017).
24. Cinti, L. & Bianchi, N. Hybrid-excited PM motor for electric vehicle. *energies* **14**, 4. https://doi.org/10.3390/en14040916 (2021).
25. Chau, K. T., Chan, C. C. & Liu, C. Overview of permanent-magnet brushless drives for electric and hybrid electric vehicles. *IEEE Trans. Ind. Electron.* **55**(6), 2246–2257. https://doi.org/10.1109/TIE.2008.918403 (2008).
26. Mohammadi, A. S. & Trovão, J. P. F. System-level optimization of hybrid excitation synchronous machines for a three-wheel electric vehicle. *IEEE Trans. Transp. Electrification* **6**(2), 690–702. https://doi.org/10.1109/TTE.2020.2992008 (2020).
27. Chu, J., Cheng, H., Sun, J., Peng, C. & Hu, Y. Multi-objective optimization design of hybrid excitation double stator permanent magnet synchronous machine. *IEEE Trans. Energy Convers.* **38**(4), 2364–2375. https://doi.org/10.1109/TEC.2023.3279934 (2023).
28. Liu, Y., Zhang, Z. & Zhang, X. Design and optimization of hybrid excitation synchronous machines with magnetic shunting rotor for electric vehicle traction applications. *IEEE Trans. Ind. Appl.* **53**(6), 5252–5261. https://doi.org/10.1109/TIA.2017.2720671 (2017).
29. Guo, Q. et al. Design and implementation of a loss optimization control for electric vehicle in-wheel permanent-magnet synchronous motor direct drive system. *Appl. Energy* **204**, 1317–1332. https://doi.org/10.1016/j.apenergy.2017.05.023 (2017).
30. Kano, Y. Design optimization of brushless synchronous machines with wound-field excitation for hybrid electric vehicles. *IEEE Energy Convers. Congr. & Expos. (ECCE)* **2015**, 2769–2775. https://doi.org/10.1109/ECCE.2015.7310048 (2015).
31. Sun, X., Jin, Z., Cai, Y., Yang, Z. & Chen, L. Grey wolf optimization algorithm based state feedback control for a bearingless permanent magnet synchronous machine. *IEEE Trans. Power Electron.* **35**(12), 13631–13640. https://doi.org/10.1109/TPEL.2020.2994254 (2020).
32. Shaier, A. A. et al. An efficient and resilient energy management strategy for hybrid microgrids inspired by the honey badger's behavior. *Results Eng.* **24**, 103161. https://doi.org/10.1016/j.rineng.2024.103161 (2024).
33. Elsonbaty, N. A., Enany, M. A. & Elymany, M. M. Hybrid permanent magnet synchronous generator as an efficient wind energy transducer for modern wind turbines. *Wind Eng.* **48**(6), 1203–1223. https://doi.org/10.1177/0309524X241256957 (2024).
34. M. Bonisławski, M. Hołub, and R. Pałka, Minimization of machine and inverter losses in hybrid excited machines for electric vehicles In *ICMEPE Conference*, 2016 Accessed Jan 19 2025. http://www.aedie.org/papers/15716-bonislawski.pdf
35. Kahraman, H. T. Metaheuristic linear modeling technique for estimating the excitation current of a synchronous motor. *Turk. J. Electr. Eng. Comput. Sci.* **22**(6), 1637–1652 (2014).
36. Gope, D. & Goel, S. K. Design optimization of permanent magnet synchronous motor using Taguchi method and experimental validation. *Int. J. Emerg. Electr. Power Syst.* **22**(1), 9–20. https://doi.org/10.1515/ijeeps-2020-0169 (2021).
37. Mörée, G. & Leijon, M. Overview of hybrid excitation in electrical machines. *Energies* **15**, 19. https://doi.org/10.3390/en15197254 (2022).
38. Wardach, M., Palka, R., Paplicki, P., Prajzendanc, P. & Zarebski, T. Modern hybrid excited electric machines. *Energies* **13**, 22. https://doi.org/10.3390/en13225910 (2020).
39. Mirjalili, S., Jangir, P. & Saremi, S. Multi-objective ant lion optimizer: a multi-objective optimization algorithm for solving engineering problems. *Appl. Intell.* **46**(1), 79–95. https://doi.org/10.1007/s10489-016-0825-8 (2017).
40. R. Mbayed, G. Salloum, L. Vido, E. Monmasson, and M. Gabsi, Hybrid excitation synchronous machine control in electric vehicle application with copper losses minimization In *6th IET International Conference on Power Electronics, Machines and Drives (PEMD 2012)* 1–6 https://doi.org/10.1049/cp.2012.0252 (2012)
41. R. Mbayed, L. Vido, G. Salloum, E. Monmasson, & M. Gabsi, Effect of iron losses on the model and control of a hybrid excitation synchronous generator In *2011 IEEE International Electric Machines & Drives Conference (IEMDC)* 971–976 https://doi.org/10.1109/IEMDC.2011.5994948(2011)
42. Shaier, A. A., Elymany, M. M., Enany, M. A. & Elsonbaty, N. A. Multi-objective optimization and algorithmic evaluation for EMS in a HRES integrating PV, wind, and backup storage. *Sci. Rep.* **15**(1), 1147. https://doi.org/10.1038/s41598-024-84227-0 (2025).
43. Mouassa, S. & Bouktir, T. Multi-objective ant lion optimization algorithm to solve large-scale multi-objective optimal reactive power dispatch *problem, COMPEL. Int. J. Comput. Math. Electr. Electron. Eng.* **38**(1), 304–324. https://doi.org/10.1108/COMPEL-05-2018-0208 (2018).

Acknowledgements

The authors extend their appreciation to the Deanship of Scientific Research at Northern Border University, Arar, KSA, for funding this research through the project number NBU-FFR-2025-2484-4, also This article has been produced with the financial support of the European Union under the REFRESH – Research Excellence For Region Sustainability and High-tech Industries project number CZ.10.03.01/00/22_003/0000048 via the Operational Programme Just Transition, project TN02000025 National Centre for Energy II and ExPEDite project a Research and Innovation action to support the implementation of the Climate Neutral and Smart Cities Mission project. ExPEDite receives funding from the European Union's Horizon Mission Programme under grant agreement No. 101139527.

Author contributions

M.M.E: Investigation, Data curation, Methodology, Software, Writing – original draft. N.A. E: Conceptualization, Supervision, Writing – original draft. A.F: Validation, Supervision, Writing- Reviewing and Editing. L.P: Investigation, Supervision, Writing- Reviewing and Editing. H.k: Supervision, Writing- Reviewing and Editing. M.A.E: Validation, Investigation, Writing- Reviewing and Editing. A.A.S: Conceptualization, Investigation, Data curation, Formal analysis, Writing – original draft.

Funding
European Union's Horizon Mission Programme, 101139527.

Declarations

Competing interests
The authors declare no competing interests.

Human and animal rights
This article does not contain any studies with animals performed by any of the authors.

Additional information
Supplementary Information The online version contains supplementary material available at https://doi.org/10.1038/s41598-025-92466-y.

Correspondence and requests for materials should be addressed to H.K.